EFFECT OF GEOMETRICAL PARAMETERS TOWARDS THE HEAT TRANSFER IN MODIFIED 80kW INDUCTION MOTOR WITH WATER COOLED DUCT

PONGSATIT ISARANKURA NA AYUTHAYA

A THESIS SUBMITTED IN PARTIAL FULFILLMENT
OF THE REQUIREMENT FOR THE DEGREE OF
MASTER OF ENGINEERING IN AUTOMOTIVE ENGINEERING
(INTERNATIONAL PROGRAM)
INTERNATIONAL COLLEGE
KING MONGKUT'S INSTITUTE OF TECHNOLOGY LADKRABANG
2014

KMITL-2014-IC-M-004-013

EFFECT OF GEOMETRICAL PARAMETERS TOWARDS THE HEAT TRANSFER IN MODIFIED 80kW INDUCTION MOTOR WITH WATER COOLED DUCT

PONGSATIT ISARANKURA NA AYUTHAYA

A THESIS SUBMITTED IN PARTIAL FULFILLMENT

OF THE REQUIREMENT FOR THE DEGREE OF

MASTER OF ENGINEERING IN AUTOMOTIVE ENGINEERING

(INTERNATIONAL PROGRAM)

INTERNATIONAL COLLEGE

KING MONGKUT'S INSTITUTE OF TECHNOLOGY LADKRABANG

2014

KMITL-2014-IC-M-004-013

APPROVAL SHEET

THESIS TITLE	EFFECT OF GEOMETRICAL PARAMETERS TOWARDS THE HEAT TRANSFER IN MODIFIED 80kW INDUCTION MOTOR WITH WATER COOLED DUCT
STUDENT	MR. PONGSATIT ISARANKURA NA AYUTHAYA
STUDENT ID	53600903
DEGREE	MASTER OF ENGINEERING
PROGRAM	AUTOMOTIVE ENGINEERING (INTERNATIONAL PROGRAM)
YEAR	2014
THESIS ADVISOR	ASSOC. PROF. DR. JARRUWAT CHAROENSUK DR.CHADCHAI SRISURANGKUL ASSOC. PROF. SEIJI OKAWA

ABSTRACT

The development of propulsion and energy storage has been implemented in electric vehicles for several years. These two critical parts are mainly faced with the thermal failure due to the operating condition; when EVs require a high power for full accelerate, it will consume a huge of electrical energy. Consequently, it will release the thermal energy to the surrounding environment where it was a waste power from the motor losses. Therefore, its improvement is focusing on the overheat prevention in particular in terms of temperature prediction in some specific areas of the motor. In the past, many studies were enhanced, researchers wrote their work to comply with experimentation. For example, apply the lump thermal network for the node's temperature prediction, the finite element analysis of the temperature gradient or even use the MATLAB to compute the theory. Thus, the history can be inferred that the studies tried to improve the studied method, and it was also to propose the idea to keep the motor temperature in operating condition. As well, this thesis will present the investigation of the cooling duct geometrical parameters towards the cooling performance. The model will use an 80kW induction motor with an inner squirrel cage rotor for the investigation. The study consisted of 3 main parts;

method verification, the simplified analysis and full-scale analysis, all of which gave around 39 sets of the result to interpret. Each set consists of temperature rising in the radius direction and the 3D contour plots which show the temperature distribution and the temperature gradient. The method verification is a hypothesis proving to ensure that the results are accurately enough. The full-scale analysis is an analysis that assumes the hypothesis to the model. However, the full-scale took too long time to analysis for 1 case. As a result, the full-scale was simplified to minimise the complexity, and it was called “Simplified analysis”. Also the simplified studied was done in 3 categories; Cooling duct width, cooling duct pitch and the base diameter of the cooling duct. Also, all of the three parts were done under the variation of cooling water flow rate; 4 litres per minute to 10 litres per minute. Moreover, the essential information of the simplified analysis will be picked for creating the prototype which it the same dimension as the full-scale model. In this studied, the prediction tool used ANSYS CFX, the method used the once which proven from other studied.

ACKNOWLEDGEMENT

This study was a master degree scholarship in automotive engineering. This program was organized by Thailand Advanced Institute of Science and Technology and Tokyo Institute of Technology (TAIST-Tokyo Tech). The course was a combination among National Science and Technology Development Agency (NSTDA), Tokyo Institute of Technology (Tokyo Tech), and King Mongkut's Institute of Technology Ladkrabang (KMITL). This research has been conducted during the year 2010-2015.

This thesis is dedicated to my grandmother, Chantana I. Lane an instructor of physics at the University of Tennessee at Chattanooga who always supported and encouraged me. Similar to all of my major advisers; ASST. PROF. DR. Jarruwat Charoensuk, Department of Mechanical Engineering, KMITL, DR.Chadchai Srisurangkul, Automotive Laboratory MTEC and ASSOC. PROF. SEIJI OKAWA, Thermal Science and Engineering Laboratory, Tokyo Tech, I am so grade, and I would like to express my thanks for everything e.g. a good advice, superb guidance, etc. I must apologise for my behaviour as sometimes I become a little aggressive toward some opinions. Apart from that, I would like to thank Mr.Dale Staniforth, who has provided guidance and support, and initially recruited me to the Bombardier Transportation where I met many great people. Further, many thanks to my team leader Ms Duangden Pentisan, who has supported me during my study. In addition, I would like to extend my appreciation to Mr. Daniel Palardy, Mr. Pasawat Lupakitaro, Mr. Winitpol Deratanapoka, Mr. Nut Panichpatana, Mr. Randula Hettiarachchi, Ms. Dilesha Herath, Mr. Chayangkun Sanguanwatana and all TAIST-Tokyo Tech members.

Finally, the success cannot happen if without my family, my father, my mother and my older brother who always gave me a suggestion as well as the financial support.

Pongsatit Isarankura Na Ayuthaya

July 2015

TABLE OF CONTENTS

PAGE

ABSTRACT I

ACKNOWLEDGEMENT III

TABLE OF CONTENTS IV

LIST OF TABLES VII

LIST OF FIGURES VIII

CHAPTER 1 INTRODUCTION 1

1.1 Background 1

1.2 Objective 3

1.3 Scopes 3

1.4 Long-term benefit 4

1.5 Research Methodology 5

1.6 Thesis Outlines 5

CHAPTER 2 RELEVANT AND LITERATURE AND THEORY REVIEWS 7

2.1 Literature Reviews 7

2.2 Overview of electric vehicle 10

2.3 Overview of an electric motor 13

2.3.1 Direct current motor 14

2.3.2 Alternating current motor 15
2.4 Principles of induction motor 16
2.4.1 Synchronous speed & Induction pole 19
2.4.2 Slip 21
2.4.3 Eddy Current Loss and Calculation 21
2.4.4 Minimum Efficiency Requirement of Induction motor. 24
2.4.5 Principles of Cooling Motor 25
2.5 Principle of Heat-transfer 25
2.6 The principle of viscous flow in pipes 29
CHAPTER 3 RESEARCH METHODOLOGY 32
3.1 Problem specification 34
3.2 Three dimension Modelling by CATIA V5 39
3.3 Method Verification 40
CHAPTER 4 FINITE ELEMENT ANALYSIS RESULTS AND DISCUSSIONS 45
4.1 Analysis Results 45
4.1.1 The result of the Full-scale model analysis 59
4.2 Results Discussion 60
CHAPTER 5 CONCLUSIONS AND SUGGESTIONS 72
5.1 Conclusion 72
5.2 Suggestion 73

Reference 74

APPENDIX A Preliminary Technical Drawing 78

APPENDIX B PROCEEDINGS 79

AUTHOR BIOGRAPHY 88

LIST OF TABLES

PAGE

Table 2.1 The relative synchronous speed toward the number of poles at each frequency..... 20

Table 2.2 The minimum efficiency of three phase induction motors under IE3 Class. 24

Table 2.3 The Reynolds number for each cooling duct width at different flow rate.. 31

Table 3.1 The material of the motor component..... 38

Table 3.2 Energy losses in the motor [33]..... 38

Table 4.1 Maximum temperatures in different components (varied by width)..... 46

Table 4.2 The maximum temperature in the different components (varied by base diameter) 52

Table 4.3 The maximum temperature in the different components (varied by pitch)56

LIST OF FIGURES

PAGE

Figure 2.1 History of EVs popularity since 1890 11

Figure 2.2 The component arrangement of the current favourite vehicle 11

Figure 2.3 Conventional type of drive train system 12

Figure 2.4 Transmission-less drive train system..... 12

Figure 2.5 Internal motor drive train system..... 13

Figure 2.6 The electric motors hierarchy..... 14

Figure 2.7 The simple mechanism and component of DM motor..... 15

Figure 2.8 A simple component of AC motor..... 15

Figure 2.9 An example of the stator laminate..... 16

Figure 2.10 The basic coil of 2 poles 3-phase induction stator..... 17

Figure 2.11 Phase angle of 3-Phase electricity 17

Figure 2.12 Rotating magnetic fields produced over simplified winding [26]..... 18

Figure 2.13 Relation Magnetic field and 3-Phase current change in 1 period..... 18

Figure 2.14 Induced current in loop creation..... 19

Figure 2.15 RMF produces a torque on a simple squirrel cage (rotor bar)..... 19

Figure 2.16 Skin effect..... 22

Figure 2.17 Skin Depth..... 23

Figure 2.18 Proximity effect 24

Figure 2.19Thermal energy transfer over the large plane wall 27

Figure 2.20 Thermal energy transfer over the contact (a: Perfect, b: imperfect) 28

Figure 2.21 A form of fluid flow in pipe at difference states 29

Figure 2.22 The phenomenon of fully developed flow in pipe 30

Figure 3.1 Flow Chart for investigation 33

Figure 3.2 (Left) The mock-up of stator body, (Right) The actual of stator body 34

Figure 3.3 (Left) A stator laminate, (Right) A stator lamina 35

Figure 3.4 A mock-up model of the stator laminate 35

Figure 3.5 A bundle of copper wire (Stator winding) 35

Figure 3.6 A single big wire (Stator winding) [32] 36

Figure 3.7 A simplified digital mock-up of winding 36

Figure 3.8 (Left) A squirrel cage (Right) An iron lamina [26] 37

Figure 3.9 The preliminary model. (Left: Rotor, Right: Stator Laminate) 39

Figure 3.10 A simplified model that show the investigation concern 40

Figure 3.11 The temperature rise in the radius direction of verified model 42

Figure 3.12 The temperature rise in the radius direction of the original model 43

Figure 3.13 A temperature contour port at the surface of the verified model 44

Figure 4.1 Trend line of maximum temperature in winding (varied by width) 47

Figure 4.2 The trending line of maximum temperature in rotor bar (width variation). 48

Figure 4.3 Trend line of pressure drop (varied by width)..... 49

Figure 4.4 Temperature distribution from the middle section of the studied model (Top Left: 5mm, Top Right: 10mm and Lower Left: 15mm)..... 50

Figure 4.5 Temperature distribution at the surface of the studied model (Top Left: 5mm, Top Right: 10mm and Lower Left: 15mm)..... 51

Figure 4.6 Trend lines of maximum temperature in winding (varied by base diameter) 53

Figure 4.7 Trend line of pressure drop (varied by base diameter)..... 53

Figure 4.8 Temperature distribution from the middle section of the studied model (Top Left: 270mm, Top Right: 280mm and Lower Left: 290mm)..... 54

Figure 4.9 Temperature distribution at the surface of the studied model (Top Left: 270mm, Top Right: 280mm and Lower Left: 290mm)..... 55

Figure 4.10 Middle plane temperature contour of the studied model (Upper Left: 15mm, Upper Right: 20mm, Lower Left: 25mm, and Lower Right 30mm).. 57

Figure 4.11 Temperature distribution at the surface of the studied model (Upper Left: 15mm, Upper Right: 20mm, Lower Left: 25mm, and Lower Right 30mm).. 58

Figure 4.12 The temperature distribution in the lateral plane of the full-scale model (Upper left: 10 L/min, Upper right: 8 L/min and Lower left: 6 L/min) 59

Figure 4.13 The temperature distribution in the longitudinal plane of the full-scale model (Upper left: 10 L/min, Upper right: 8 L/min and Lower left: 6 L/min) 60

Figure 4.14 Heat Flux in direction out of Rotor Conductor Bar 61

Figure 4.15 The perpendicular line on the curve 61

Figure 4.16 Heat Flux of Rotor Region..... 62

Figure 4.17 Heat Flux of Stator Winding 62

Figure 4.18 Heat Flux in direction to the Stator Wedge (plus value) 63

Figure 4.19 Heat Flux in direction out (minus value) of Stator Wedge 63

Figure 4.20 Heat Flux in direction out (minus value) of Stator laminated 64

Figure 4.21 Heat Flux in (Blue) and out (Red) of Stator Jacket..... 64

Figure 4.22 Temperature distribution in the middle section of the Stator Jacket..... 65

Figure 4.23 Temperature distribution in the middle section of the Stator Jacket and body..... 65

Figure 4.24 Temperature distribution in the middle section of the Stator (Maximum scale at 56.32℃)..... 66

Figure 4.25 Temperature distribution in the surface of the Stator (Maximum scale at 76.56℃) 66

Figure 4.26 Temperature distribution in the surface of the rotor 67

Figure 4.27 Temperature distribution in the surface of the rotor in different widths (Top Left: 5mm, Top Right: 10mm and Lower Left: 15mm)..... 68

Figure 4.28 Heat Flux of Rotor Region in different widths (Top Left: 5mm, Top Right: 10mm and Lower Left: 15mm)..... 69

Figure 4.29 Temperature distribution in the surface of the rotor in different widths (Top Left: 5mm, Top Right: 10mm and Lower Left: 15mm)..... 69

Figure 4.30 Heat Flux in (Blue) and out (Red) of Stator Jacket in different width (Top Left: 5mm, Top Right: 10mm and Lower Left: 15mm) 70

Figure 4.31 Heat Flux in direction out of Stator Jacket in different width (Top Left: 5mm, Top Right: 10mm and Lower Left: 15mm)..... 71

CHAPTER 1
INTRODUCTION

1.1 Background

Since the electro-mechanical machine invention in the early 19th century, it has been continuously developed for the benefit of manpower, enhancement in productivity rate and taken part in transportation revolution. In the mid 19th century, during the second industrial revolution, people began to use it in some applications such as the replacement of the heavy machine from a steam engine to an electric motor. Similarly, it was used in transportation application by replacing locomotive propulsion. Therefore, instead of steam driven pistons, the traction motor bogie was introduced. However, due to its limitations and technologies, for example, the mobility of energy storage, it was not accepted as much as it should have at that time. Therefore, the people continued to consider fossil fuel as a primary energy source for vehicle movement. Even though electric propulsion was not the preferred energy source, it was still useful in some particular places. For example for confined space application such as at mines, it is vastly beneficial and safe as electricity, and it does not produce any toxic gases.

At the same time in the automobile industry, there were three different drive systems, namely the steam engine, the gasoline engine and the electric motor. Unfortunately, the electric driven system was not the chosen solution. Thus, it had to wait for another century until it was introduced again recently. By then it has gone through several key developments such as the energy storage system had been improved from non-rechargeable to rechargeable batteries. Similarly, the propulsion system had been enhanced to increase the motor power. Even though the improvement in power seems to be a problem free solution, the electric motor still had a little problem on the losses [1]. As a result, the temperature rose inside the motor.

Despite the fact, it has had some issue with the electrical propulsion failure, the improvements were worth carrying out when considering the efficiency, which served better on the environment. Therefore, it was essential to be protected from the overheating failure; otherwise all the developments will be useless. Hence, the statistics had revealed; the electrical failure had contributed about 80%, and the bearing failure was about 20% [2]. The bearing failure can be fixed by replacing with a new part at the end of its lifetime. However, the electrical failure has two option for improvement; 1) By increasing the efficiency to reduce the losses and 2) By removing the waste energy from the motor. Especially, when the motor is used in an electric vehicle, it requires high power in the form of high electrical current and high voltage to meet the specific power requirements. Unfortunately, its temperature shall rise greater than those in other applications [3]. Furthermore, most of the existing models uses an old-fashioned design where the cooling system was estimated based on the idea of trial and error. When considering the long-term effects, the conventional design will reduce its efficiency and it might have a chance to face with the thermal damage. From the statistic, the biggest issue about the failure is the overtemperature at the stator winding.

The temperature prediction shall be analysed by using computer aided engineering tools (CAE). The results that were used for analysis are similar to those obtained from the experiments that required the real prototype to perform the test while CAE requires "digital mock-up" for performing the same analysis. The benefits of using CAE; 1) Reducing the mistake during the test 2) Reducing the development timing and 3) Reduce the cost. However, CAE is similar to experiment, if a user does not understand their studied model, hypothesis and the problem specification, the result shall be inaccurate. Therefore, the user should be reminded that the hypothesis and the problem specification must be clearly clarified before performing the analysis.

The model being investigated in this study is the 80 kW induction motor with an inner squirrel cage rotor enclosed by a water-cooled path. The studied shall focus on the cooling performance. The mock-up model shall be created by using CATIA V5.

The study shall vary the width, the base diameter and the pitch length of the cooling duct. The duct has 5 mm height, and for investigation the width shall be adjusted from 5mm to 15mm. Moreover, the cooling path was made by machining at the surface of the stator body. Therefore, the cooling path shall be relied on the body diameter. On the other hand, for study the cooling path shall be changed its diameter or the base diameter from 270mm to 300mm. Also, the pitch length was made by machining, so the pitch was the other variable that shall be investigated. The length shall be changed from 15mm to 30mm. About eight models shall be created from CATIA V5, and every model shall be examined under different flow rate. Flow rate shall be varied from 4 litres per minute to 10 litres per minute. Therefore, about 32 cases shall be performed the temperature analysis by ANSYS CFX. However, the investigation by using full-scale mock-up shall not suitable for this study due to the limit of time. Consequently, the mock-up shall be reduced to a simple model (Simplification method) to complete the study.

1.2 Objective

1) To investigate the temperature distribution including the hot spot in the induction motor by; varying the cooling duct geometry and adjusting the water flow rate.

2) To use “ANSYS CFX” for solving the problem, monitoring the temperature rise in the motor component, analyse the result and evaluate of reliability of the results.

3) To publish the data and use it as a guideline for new generation designer to investigate under more comprehensive of the multi-physic model.

1.3 Scopes

1) Digital mock-up shall be created following the 80kW induction motor with squirrel cage rotor and water-cooled surface.

2) The Investigation shall focus on the geometry and the cooling water flow rate toward to the temperature rise in the motor.

3) The geometrical investigation shall split into four sections. The cooling duct width shall be varied from 5mm to 15mm. The cooling duct base diameter shall be changed from 270mm to 290mm. The cooling duct pitch length shall be modified from 15mm to 30mm. The last, the full-scale model shall be created and analysed.

4) The relation among of cover, rotor and bearing shall be assumed to be concentricity.

5) "ANSYS CFX" shall be used to predict motor temperature.

6) The studied assumes that 40% of peak power is total losses.

7) The results shall mainly focus on the temperature in stator winding.

1.4 Long-term benefit

1) The studied results shall be used as a guideline for the future design.

2) The method of the study is for guidance, and it can be applied to the other related analysis in the future. (Note: losses ratio depends on the type of motor.)

3) The large-scale induction motor will spend shorter development time than the previous after applying CAE.

4) In the future, the designer can expand the analysis scope to multi-physics level; for example, electromagnetic analysis coupled with thermal analysis. (Note: the thesis uses the thermal analysis model only.)

1.5 Research Methodology

1) Problem Specification; the solution, method, and the investigation topic.

2) Create mock-up model by using CATIA V5.

3) Verify the studied method.

4) Perform models analysis.

5) Summary and interpret the results.

6) Conclude all the results.

1.6 Thesis Outlines

The thesis has 5 Chapters; all of the contents are summarised as followed:

Chapter 1: Introduction

This chapter briefly describes the motor usage and identify its current issues, including the objective, scope and hypothesis. Besides that, the long-term benefit and the method sequence shall be presented.

Chapter 2: Relevant literature and theory reviews

This chapter mainly focuses on the former studies and relative knowledge. For example, literature reviews the principle of EVs, electric motor and the theory of heat transfer and fluid mechanic.

Chapter 3: Research Methodology

This chapter describes the sequence of study, shown by a flowchart.

Chapter 4: Finite element analysis results and summaries

This chapter shows the results; 32 cases from the simplified studied and 3 cases from a full-scale model studied. Summarization of all results will be completed at the end.

Chapter 5: Conclusion and suggestions

This chapter concludes the crystallisation of the summaries in chapter 4, including comments about the study in the last chapter as well.

CHAPTER 2

RELEVANT AND LITERATURE AND THEORY REVIEWS

2.1 Literature Reviews

The main reason that motor temperature estimation becomes interesting is due to the damage that is caused by thermal overload during operation. Therefore temperature needs to be considered as a main parameter. The damage relies on the winding insulation class. For example, instead of using the winding insulation class H, using class B under the maximum temperature at 180 °C, the lifecycle will reduce to 1800 hours. Therefore, the selection should follow the electronic insulation system (EIS), to avoid the motor from thermal damage [4]. Also, during the mid-1930s, V.M. Montsinger discovered the behaviour of isolating material at the over temperatures condition. He found that when the load over the limitation, the life age of isolating material shall reduce its lifespan by a half. For this reason, the temperature prediction and the located estimation shall be an essential topic to do a study. In general, the temperature prediction has been done by two methods; 1) Using the lump thermal network model and 2) Using computer aids engineering (CAE).

In 1991, the lump thermal network was used to estimate the temperature of A Totally Enclosed Fan-Cooled electric motor (TEFC) [5]. Many years later, Boglietti and the team used the network model to predict the temperature in the motor component. The network was created by converting the 4kW- four poles induction motor into the simple form of the model. Their prediction method did the calculation under; 1) Used the steady state condition. 2) Centre of the shaft in the radial direction was assumed to be asymmetrical. 3) An asymmetrical temperature at the external fan mounted region was neglected. 4) The heat sources were uniformly distributed. 5) The heat flux in the axial direction was considered only in the shaft. 6) The convective resistance between the external frame and the ambient was assumed to be variable. Moreover, their thermal model was verified by the experiment, and it succeeded. The lump network results had a fluctuation of temperature around ±5 °C when compared to the temperature of the experiment.

The experiment was set up by placing four temperature sensors at different locations for temperature monitoring. Three sensors attached to the external connections of the stator windings and one sensor installed in the stator yoke [6]. Two years later, the AeroVironment's motor (75kW TEFC Induction motor) was converted to the thermal network by Baggu and his colleagues. They proposed the technique that adding the capacitances nodes to the diagram; the technique improved the accuracy of the thermal network model. As a result, it produced the satisfied outcome. Furthermore, the technique also enabled the network to predict the temperature at different power states [7]. In fact under the real situation, the voltage supply could be not stable, and it shall be a cause of the thermal issue. For example in 2010, some studied did the investigation of the unbalanced voltage by using the network. The prediction result gave the fluctuation of temperature about 9% to 13% when compared with the experiment. The losses in their model were calculated. The losses in difference location were following; a stator, a rotor iron, a rotor and a mechanical had 1600W, 618W, 620W and 460W respectively [8].

In 1996, the ability of CAE can serve only 2D analysis because the limitation of computer hardware. Lee and his colleague used CAE for predicting the temperature. The heat sources for the programme set up were calculated by Maxwell's electromagnetic and Kirchhoff’s current equations. The heat sources were following; Rotor Bar 40.24%, Stator Winding 27.27%, Stator teeth 28.53%, Stator Yoke 3.90% and Rotor teeth 0.06%. The finite element analysis gave two types of the result; first is the temperature distribution in 2D contour plot and the other is the temperature along the radius direction. Both results show that the highest temperature is in the rotor bar region [9]. Next year, Lampard and the team challenged the predicting technique by using the 3D technique, but at that time the computer was not fast as the present. Therefore, they proposed to use a mesh-sliding technique to reduce the computing time [10]. In 2006, Ying and the other estimated the temperature of the model under the condition that the rotor bar broken (Under the thermal stress operation, the rotor bar might be broken). Their studied was applied the coupled technique (the combination of magnetic analysis and thermal analysis). Their effort

into the technique was proven by the experimental verification. Finally, the method was useful, and it can estimate the temperature under the effects of rotor bar broken as well [11]. At the same year, Nakahama and his team successfully predicted the temperature of airflow through a ventilation path (Fin) of a motor (open-type). Their prediction was proven by mock-up model which shown the flow direction [12]. One of the best things of CAE is that it can predict the temperature in every type of motors, based on the essential parameter for a program that matches with the analysis or not. Zhang and the others, they studied the phenomenon of the temperature change toward the varying load adjustment. The studied use the permanent magnet synchronous motor (PMSM) 30kW and, the temperature analysis was done on the 2D model. During the analysis, the motor power was changed, varying between 50% to 100% of the duty. As a result, the relationship between the power and the temperature of the rotor core and rotor bar rose as a linear [13]. Many studies give more involve of CAE and CFD in the analysis; it can predict the wind temperature along the housing fin. Therefore, the study of housing shape also has significance on the heat transfer ability [14]. Then in 2011, the study of a simplified 3D model in the static temperature field had been presented by Cuiping and his team. They investigated the role of temperature rise in the motor after changing the water flow rate. The analysis results showed that the highest temperature located in the rotor bar region, and the air gap had an influential effect on the thermal transfer ability [15]. Later on, in 2012 Baptista and the team applied the same method to the eccentricity of the motor. An induction motor with 0.28 mm nominal of the air gap was converted to the network model, and the study was done under the variation of the misalignment in the radius direction. The ratio between the upper air gap and the lower air gap following: 0, 3/6 (0.14 mm), 5/6 (0.233 mm). The result shows that the more misalignment, the more rising in temperature, because the higher of misalignment ratio creates a huge air gap. Consequently, the air gap makes the difficulty to the electromagnetic energy cross over the gap, so the air gap is one of the primary factors for thermal damage [16].

Besides, the researcher can use both the thermal network and CAE technique to predict the temperature. These give the similar results, but the CAE can show the temperature in some particular area [17]. Also, the thermal network represents the temperature even in the three dimensions. JinXin and team created three dimensions thermal network method by converting to the 2D diagram. This method was easier than using 3D FEM. However, they found that the FEM aids them to monitor the temperature inside the PMSM instead of showing only the surface temperature or the node temperature [18]. Moreover, the thermal network can apply to the SIMULINK and MATLAB, and it allows the model to be more complex [19].

Finally, all of these studies can be inferred as below; 1) Both methods have been improved for enabling the temperature prediction in three dimensions. 2) Both methods have been enhanced for supporting the thermal prediction in a diverse range of motors. 3) CAE illustrates the temperature in every location of the motor. 4) Both methods improve the technique for predicting the housing shape concerning the heat transfer. Therefore, this thesis shall investigate the effect of geometrical parameters towards the heat transfer in the modified 80kW induction motor with a water-cooled path.

2.2 Overview of electric vehicle

The electric cars were comfortable, quiet, clean, and fashionable. It also does not require transmission gear and is easy to control. The electric motor was used as propulsion to accelerate or decelerate, and use as chemical batteries for energy storage. However, in the historical time the usage was limited by the capacity of the battery. They were suitable only for the city usage and after every trip, the battery needed to be charged again. The electric cars era started since 1890 as shown in Figure 2.1. Until now, six types of electric vehicles have been developed. The first vehicle used a pure electric motor consisting rechargeable batteries only. The second used a combination of electric motor and internal combustion engine, mostly known as hybrid vehicles. The third type is similar to the first, but an extra device such as fuel cells supplies the energy. The fourth is the vehicle in which the

energy is provided by power lines, as seen in a tram while the fifth are the solar energy vehicles. The last is similar to the first and the third types. However, the energy was stored in an alternative form such as flywheels or super capacitors [1], [20] & [21].

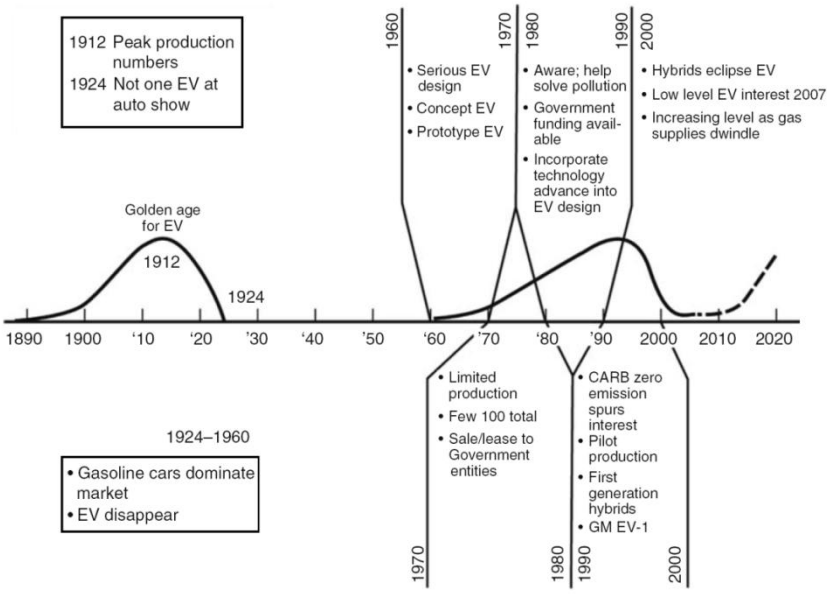

Figure 2.1 History of EVs popularity since 1890

In the present, only three types of personal vehicles are being used, they are a pure electrical type, a pure internal combustion engine (IC engine) type and a hybrid type. The components arrangements of each type shown in Figure 2.2.

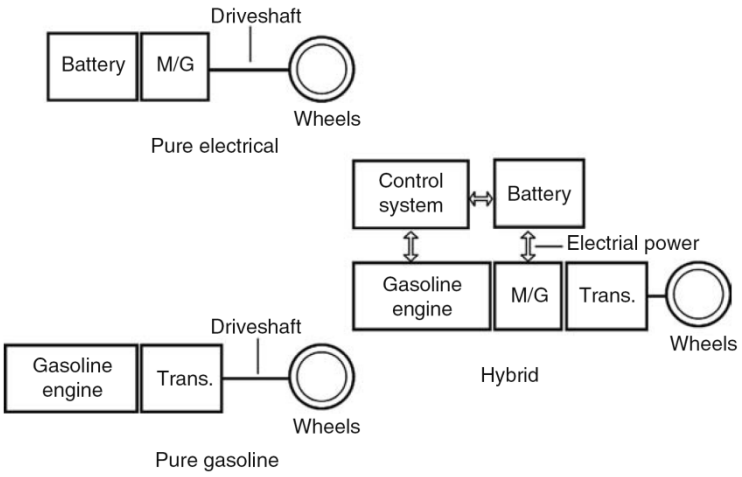

Figure 2.2 The component arrangement of the current favourite vehicle

The component arrangement of a pure electrical type, the vehicle shall be in many forms depending on the type of the electric motor [22]. They can be categorized into three main types. The first is the conventional type, where an IC engine is replaced by an electric motor, which transmits power through transmission gears as shown in Figure 2.3.

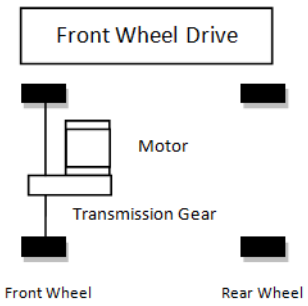

Figure 2.3 Conventional type of drive train system

The second consists of an electric motor, which connects to the driving shaft directly. It is called as "Transmission less", where the motor shaft connects to the reducing gear, to reduce the revolution speed as shown in Figure 2.4.

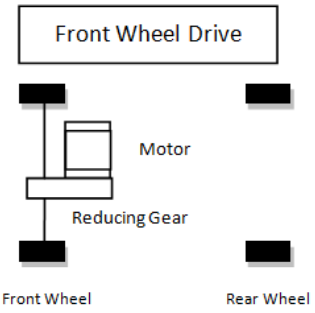

Figure 2.4 Transmission-less drive train system

The last type is similar to the four-wheel drive cars where every wheel enforces the vehicle movement. An in-wheels drive system installs the motor to the wheel directly. It will reduce the component of the vehicle because it does not need any shaft to drive the vehicle. The configuration is demonstrated in Figure 2.5.

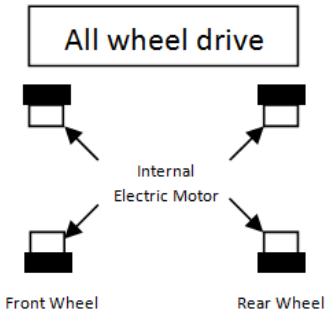

Figure 2.5 Internal motor drive train system

The difference between the motor configuration influences to the motor selection. For example if the internal combustion car needs to retrofit the propulsion system, induction motor or PM motor should be selected for replacing.

2.3 Overview of an electric motor

A machine that converts electrical energy into mechanical energy is called an electrical motor while the device that converts mechanical energy to electrical is known as a generator. When a motor is used, the machine operates via a magnetic field that is produced by the electric current. This magnetic field also creates the mechanical force throughout the rotor shaft. On the other hand when using a generator, the reversible process will occur [23]. In some applications, the electromagnetic machine is possible to be both, motor and generator when it was used. For example, the automobile propulsion, which is driven by the motoring mode and braking by the regenerative electricity. In most applications, it is used as a driver (motor). Examples are Industrial fans, blowers and pumps, machine tools, household appliances, power tools, and disk drives. The device is available in both electrical sources of energy; direct current (DC) and alternating current (AC). Also, it is available in a variety of size, such as from a motor in a watch to the giant ship propulsion. Therefore, the types of an electric motor can be grouped as shown in Figure 2.6.

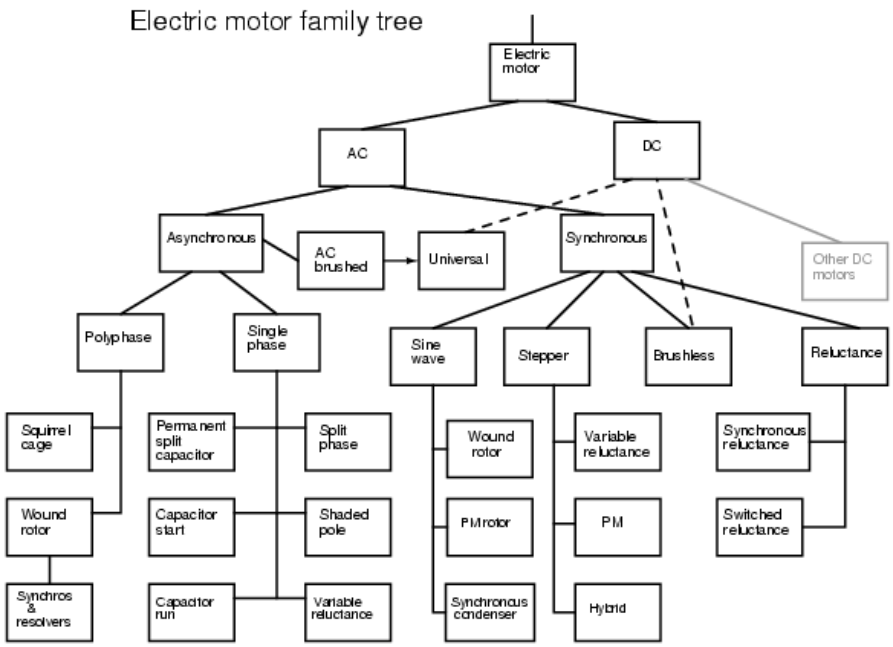

Figure 2.6 The electric motors hierarchy

2.3.1 Direct current motor

Direct Current Motors (DC motor) is operated by the DC energy. The speed shall be controlled via using either a variable supply voltage or by changing the strength of the current. A simple DC motor has a stationary set of permanent magnets in the stator and an armature (rotor) with the windings of insulated wire wrapped around a soft iron core. It usually has multiple turns around the core and the ends winding are connected to a commutator. It allows each armature coil to be energized in turn and connects the rotating coils with the external power supply through brushes. The simple mechanism of rotation shown in Figure 2.7.

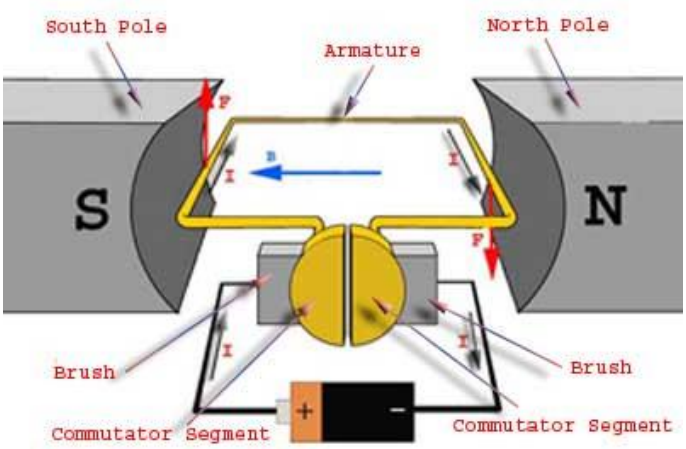

Figure 2.7 The simple mechanism and component of DM motor

2.3.2 Alternating current motor

The alternating current (AC) induction motors and synchronous motors are the most widely used in the industry due to it is rugged, reliable and economic benefits. They are also available in a variety of size, from the small size as a servo-motor in pneumatic systems, to the large size as a main rolling stock propulsion or electric vehicle propulsion. The frame, stator, rotor and bearing are the standard part of every motor as shown in Figure 2.8.

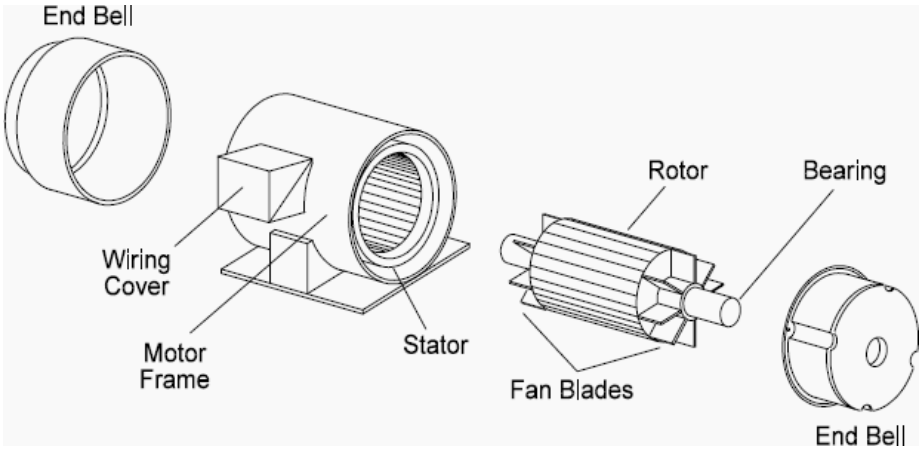

Figure 2.8 A simple component of AC motor

However, the essential components of an AC induction motor are, the stationary or static component (Integration of frame and stator) and the rotating component

called rotor. The stator is made from the laminations of high-grade steel sheets, where the inner surface are cut into slots as shown in Figure 2.9 for the accommodate windings conductor [24]. In the past, the slotted stators did not exist. Thus, the original stator was made from induction coil as shown in Figure 2.10.

Figure 2.9 An example of the stator laminate

Unlike synchronous, the induction motor does not require mechanical commutation to stimulate the revolving mechanism. The rotor can be either wound type or squirrel-cage type, the most widely used in the industry is the Three-phase, squirrel cage, induction motors. However, the angular speed of the motor depends on the frequency. The frequency can be increased by using variable-frequency drives (VFDs). These devices offer a significant key to energy savings and an opportunity for existing and prospective induction motors to be available in variable torque too.

2.4 Principles of induction motor

A simple model of an induction motor (Figure 2.10) will be used. The magnetic inductance (due to the current flow) is a causes the rotation of the rotor. For a synchronous motor, the rotor turns at the same rate as the stator field, whereas, for the induction motor, the rotor turns slower than the stator [24] & [25].

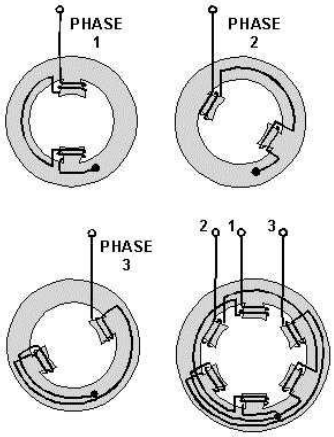

Figure 2.10 The basic coil of 2 poles 3-phase induction stator

The AC three phase electricity has a 120° differentiation of phase along the Voltage line 1(V1) Voltage line 2(V2) and Voltage line 3(V3). The phenomena of magnetism in a conductor wire shall induce the magnetic field follow the right-hand rule. During the electric current change the phase; the magnetic field direction shall be inverted. The relation between voltage change and the time in one cycle shown in Figure 2.11.

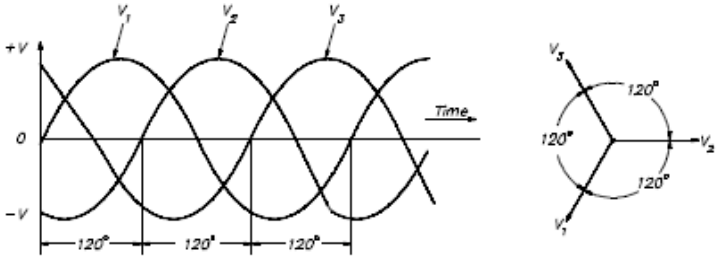

Figure 2.11 Phase angle of 3-Phase electricity

Thus, when using three conductor wires (Figure 2.12), each wire shall energize a magnetic field. When combining magnetic fields together, it will create a new form of magnetic field (same pole with Constructive Interference, the opposite pole with Destructive Interference).

Figure 2.12 Rotating magnetic fields produced over simplified winding [26]

As a summary, the relationship between magnetic field towards the current phase change of 3-phase in a period is illustrated in Figure 2.13.

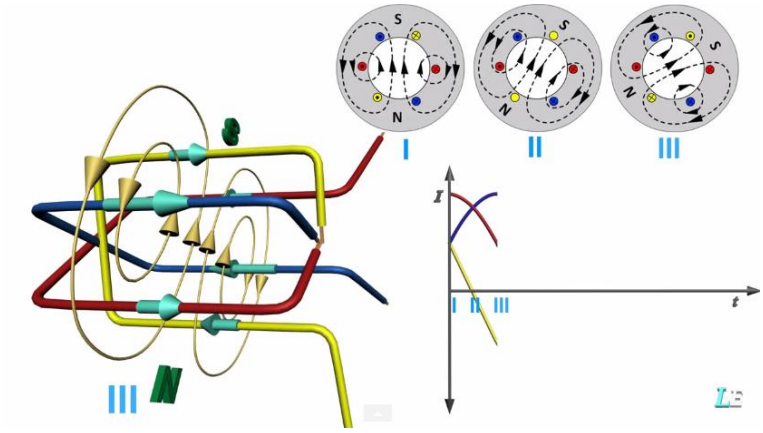

Figure 2.13 Relation Magnetic field and 3-Phase current change in 1 period

When considering the rotor mechanism, only a little knowledge is required. First, similar to the stator, when the magnetic field is created inside, it will induce current in rotor loop that is indicated by the transparent blue arrow in Figure 2.14.

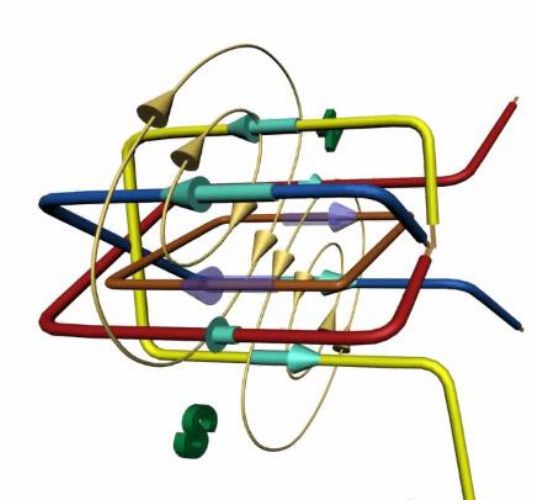

Figure 2.14 Induced current in loop creation

The second concept that can be used to describe the function of the rotor is the theory of Lorentz force. This theory states that when a wire carrying an electrical current is placed in a magnetic field, it will create a force on the wire. Thus, a force shall be energized on the squirrel cage bars as shown in Figure 2.15.

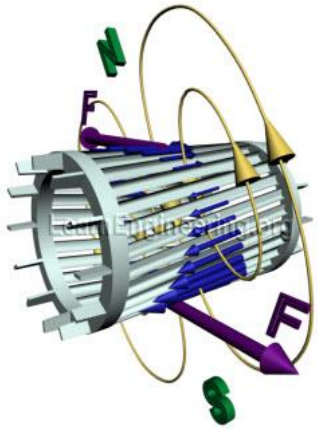

Figure 2.15 RMF produces a torque on a simple squirrel cage (rotor bar)

2.4.1 Synchronous speed & Induction pole

This section will brief about rotor movement speed. As explained in previous sections, the induced magnetic by voltage and phase angle differences will result in rotation of the rotor. Since the 3-phase electricity is dependent on frequency, it can

be inferred that the rotor movement is about 3-phase electricity. The magnetic field speed in the stator is called synchronous speed, and it can estimate by equation 2.1.

$$N_s = \frac{120f}{p} \tag{2.1}$$

In this equation, Ns is the synchronous speed, f is the electricity frequency, and p is the motor pole. Table 2.1, the relation of synchronous speed about the number of a pole at the variation of frequency is illustrated.

Table 2.1 The relative synchronous speed toward the number of poles at each frequency

Pole Number	Synchronous speeds, in Rev/min					
	50 Hz	60 Hz	70 Hz	80 Hz	90 Hz	100 Hz
2	3000	3600	4200	4800	5400	6000
4	1500	1800	2100	2400	2700	3000
6	1000	1200	1400	1600	1800	2000
8	750	900	1050	1200	1350	1500
10	600	720	840	960	1080	1200
12	500	600	700	800	900	1000

2.4.2 Slip

The previous section described the rotor rotating mechanism, which has proven that the rotor rotating speed is related to the rotating field in the stator. However, if the rotor is stationary and the rotating field cut the rotor bar at synchronous speed (high relative velocity with respect to the rotating field), will result in high E.M.F. On the other hand if the rotor operation speed is same as synchronous speed, the relative velocity with respect to the rotating field is zero, then there is be no E.M.F. induced in the rotor bar. The relative speed between the rotor and the field is known as "Slip". If the rotor operation speed is "N" and rotating field (synchronous) speed is "Ns", the slip speed will be "Ns - N". Therefore, the slip ratio is the relative of slip speed to the synchronous speed as shown by equation 2.2 [27].

$$S = \frac{N_s - N}{N_s} \tag{2.2}$$

2.4.3 Eddy Current Loss and Calculation

The eddy currents arise from a change of magnetic field in winding. The current does not flow in the centre of the conductor but increases at the skin of the conductor.

2.4.3.1 Copper losses

A copper loss in the machine winding occurs when currents flow through the winding. Hence, energy is dissipated by the resistance of the conductor, which leads to the following heat effect in a conductor. The level of heat transfer in winding depends on the cross-sectional area and the length of the conductor.

Copper loss is directly proportional to currents passing through the wire, which can be obtained by the square of the currents flowing in the conductor and its resistance as written in the equation below.

$$P_{Cu} = I^2R \tag{2.3}$$

2.4.3.2 Skin Effect

The skin effect is associated with the distribution of current in a conductor. The current distribution peaks at the surface of the conductor with large current densities and gradually decreases at depth. The skin effect is related to the rate of change of magnetic fields within the wire, which leads to the phenomenon of eddy currents. Furthermore, the effective resistance is one major factor in the skin effect when the frequency is increased.

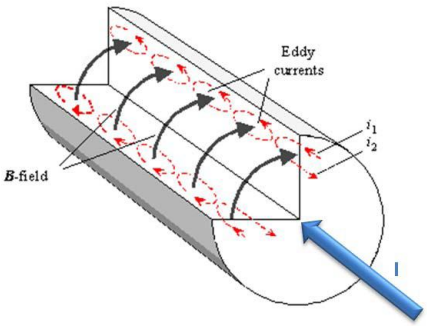

Figure 2.16 Skin effect

2.4.3.3 Skin Depth

The distance between the surface and the skin of the conductor level is called the skin depth. The distance of skin depth is inversely proportional to the square root of frequency.

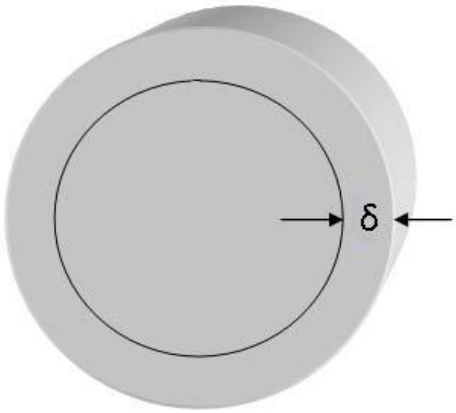

Figure 2.17 Skin Depth

$$\delta = \frac{1}{\sqrt{\pi f \sigma \mu}} \tag{2.4}$$

2.4.3.4 Proximity Effect

The proximity effect is an effect on an external magnetic field, which has been generated by currents flowing in other nearby conductors or the other environment. The external magnetic field will perturb the current distribution and induce eddy currents in the nearby conductors.

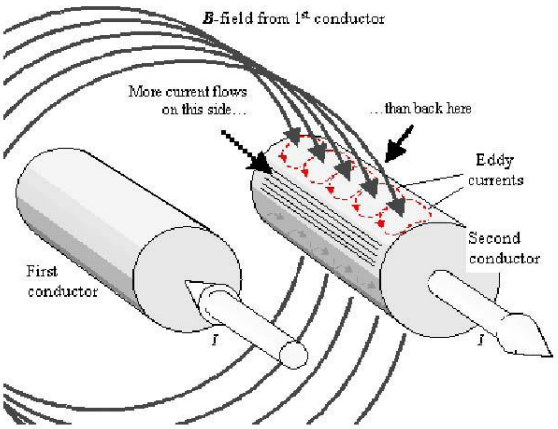

Figure 2.18 Proximity effect

2.4.4 Minimum Efficiency Requirement of Induction motor.

Regarding IEC standard No.60034-30 part 1, the committee attempted to force motor manufacturers to implement a high-efficiency motor. New adoption of the norm will force every manufacturer to improve their product performance to meet with the IE3 class efficiency by January 1, 2015, for 7.5 to 375 kW [28].

Table 2.2 The minimum efficiency of three phase induction motors under IE3 Class.

Rate Power (kW)	Efficiency (%)
30	92.7
45	93.4
55	93.7
75	94.2
90	94.4

The assessment can be performed in two ways, firstly by performing a test, and the other is by calculation. In general, the efficiency is the comparison between input power and output power as shown by equation 2.5 [21].

$$\eta_m = \frac{\text{Output power}}{\text{Input power}} \tag{2.5}$$

On the other hand, input power is the output power combined with the loss.

$$\eta_m = \frac{\text{Output power}}{\text{Output power} + \text{Loss}} \tag{2.6}$$

2.4.5 Principles of Cooling Motor

The previous section described energy loss. Hence, to minimize this loss, the motor needs to operate with maximum efficiency. Therefore, the temperature is a vital parameter that must be taken into account. Otherwise, the electric motor could be damaged. To remove the excess heat and to maintain the process under operating temperatures, the cooling system should be calculated to overcome the excess heat generation. In general, only two types of cooling systems are used. The "Air cooling" system will install turbines on the shaft of motors to reduce the heat of motors by blowing the wind through the fin. The fins are integrated with a housing that behaves similarly to a heat sink. However, in "Water-cooled" system, the cooling conduit is integrated with the motor housing, which feeds the cooling fluid through the conduit. The temperature of all the components could be reduced by using this system. Thus, the liquid cooling is better than air-cooling in term of temperature that efficiency improves by 1% [21].

2.5 Principle of Heat-transfer

About the theory of thermodynamics, heat transfer can be described as the mechanism for energy conservation between physical systems. The principal modes of heat transfer are consisting of 1). Conduction, 2). Convection and 3). Radiation [29]. However, the mechanism of heat transfers still need to follow the first law of thermodynamics. The energy conservation, states that the total energy of an isolated system, the energy can be transformed from one form to another as describes by equation 2.7 [30].

$$\Delta E^{tot} = \Delta E^{kin} + \Delta E^{pot} + \Delta U \quad (2.7)$$

Where, ΔE^{tot} is the rate of change in term of total energy. ΔE^{kin} is the rate of change in term of kinetic energy. ΔE^{pot} is the rate of change in term of potential energy, and ΔU is the rate of change in term of internal energy. In the case that the energy changes from electric energy to thermal energy and mechanical energy, the equation 2.7 can be rewritten as shown by the below equation 2.8.

$$E = Q + W \quad (2.8)$$

Where, E is energy input (electrical energy), Q is thermal energy and W is work output or mechanical energy.

Conduction, which occurs as a result of interactions between the particles, is the transfer of energy from high energetic particles to the lower energetic particles. This phenomenon occurs in all solids, liquids, or gases. In solids, the conduction occurs via the combination of molecule vibrations in a lattice and the energy is transported via free electrons. On the other hand, in gases and liquids conduction occurs via the collisions and diffusion of the molecules during their random motion. The conduction rate depends on the geometry, thickness, the material of the medium and the temperature difference across the medium. It also can infer that the rate of heat transfer through the wall is doubled when the temperature difference between the wall or the area normal to the direction of heat transfer is doubled. However, the transfer will drop to half when the wall thickness is doubled. Thus, when the medium is a large plane wall with thickness "L" and area “A”, the temperature difference across the wall is $\Delta T = T_2 - T_1$ as shown in Figure 2.19 [29].

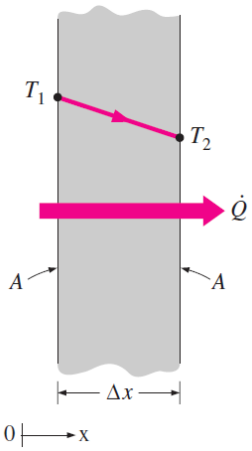

Figure 2.19Thermal energy transfer over the large plane wall

The rate of heat conduction ($\dot{Q}_{cond}$) can be expressed as the below equation 2.9.

$$\dot{Q}_{cond} = -kA\frac{dT}{dX} \tag{2.9}$$

Where, "k" is thermal conductivity. Each material consists of difference thermal conductivities (For example iron is 80.2 W/m•°C, Water (l) is 0.613 W/m•°C at room temperature).

An ideal conduction is when two difference materials contact it can perfectly transfer the thermal energy from one side to the other without leaving any energy. In fact, when two difference materials contact, the roughness will make the air gap that act as insulation to resist the thermal energy as shown in Figure 2.20, this resistance is called the thermal contact resistance.

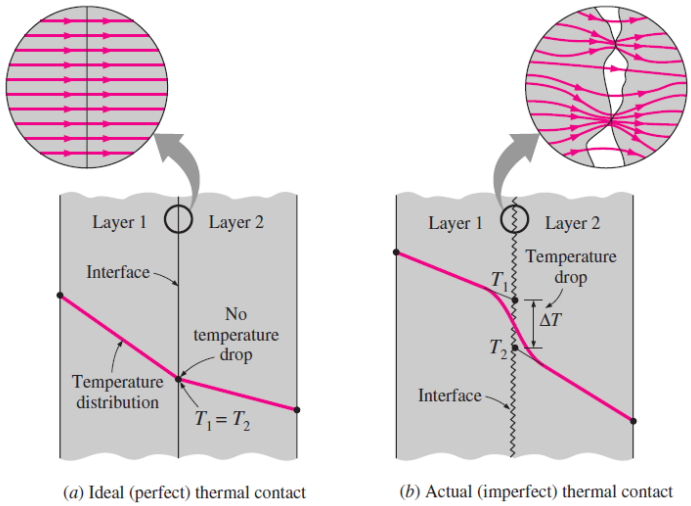

Figure 2.20 Thermal energy transfer over the contact (a: Perfect, b: imperfect)

Next, convection is the translation of energy between a solid surface and the enclosed liquid or gas. The energy in the solid surface must be same as the energy that is transferred to the enclosed liquid or gas, which could be rewritten as shown in equation 2.10.

$$\dot{Q}_{conv} = hA_s(T_s - T_\infty) \tag{2.10}$$

Subsequently, radiation is the energy emitted by matter in the form of electromagnetic waves (or photons) which is a result of the changes in the electronic configurations of atoms or molecules. Unlike conduction and convection, the transfer of energy by radiation does not require any medium. In fact, the energy transferred by radiation is fastest (at the speed of light) and it suffers no attenuation in a vacuum.

Finally, when the conjugate heat transfer or the heat transfer of the solid domain and fluid domain are calculated simultaneously, the conservation of energy equation will combine the equation of conduction, convection and volumetric.

2.6 The principle of viscous flow in pipes

The principle of viscous flow in pipes shall be described by the governing equation. It concerns about mass, momentum, and energy conservation. The fluid flow in a closed path is crucial for many applications and several of sizes. For example bloodline, a man-made Alaskan pipeline for crude oil, conveying system or the engine cooling system. Although all of these applications are different, the principles of governing the equation are the same. Before moving to the governing equations, the concepts of pipe flow will be described first.

Although, several types of conduits are used to transport fluid; duct profiles are the most preferable. Typical circular channels are designed to withstand a considerable pressure difference across their walls without undue distortion of their shape. Nevertheless, non-circular conduits are often consists of rectangular cross sections. Typically the pressure difference between the inside and outside of these ducts is relatively small. Most of the principles involved are independent of the cross-sectional shape. However, the details of the flow may be dependent on it unless the conduit was assumed to be relative a round shape channel. The fluid flow in a pipe could be categorized into three possible flow types, namely laminar, transitional or turbulent flow, which is dependent on the conduit diameter and average fluid flow rate. Figure 2.21, at point A, if the measured velocity against time is constant, this flow is known as "Laminar". If it tends to vary between being steady and irregular, it is called "Transitional" and if the variation happens all the time, it is called "Turbulent".

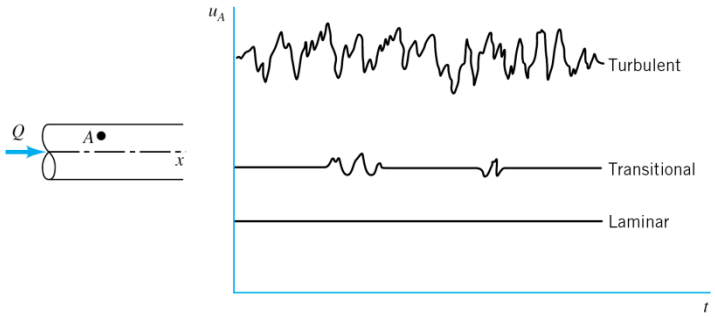

Figure 2.21 A form of fluid flow in pipe at difference states

Additionally, the fluid motion in the pipe is flow in the turbulent state, and it enhances the energy transfer between particles. As a result, the convection rate shall be enhanced from this activity. Typically, when the fluid flows in pipes, it has two regions. At the beginning of the pipe is called the entrance region flow, in this state, all properties are not in the stable value. Therefore, when calculating the next to region shall be used that is the fully developed flow, as shown in Figure 2.22.

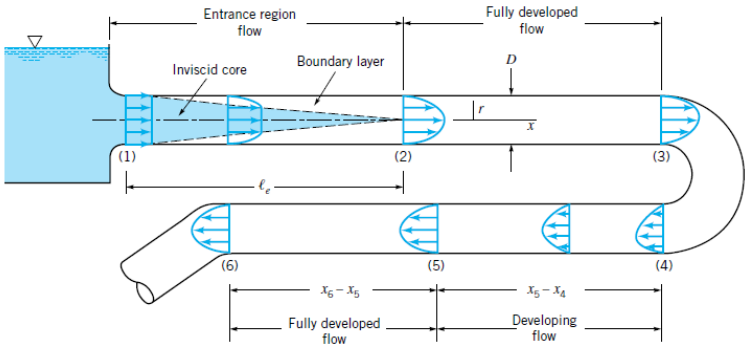

Figure 2.22 The phenomenon of fully developed flow in pipe

The flow in a pipe during its fully developed region is possible to be laminar or turbulent, depending on the value of the "Reynolds number". For a pipe flow, the value of the Reynolds number must be approximately less than 2100 for laminar flow and greater than 4000 for turbulent flow. The Reynolds number might be calculated by using the following equation 2.11.

$$\boldsymbol{Re = \frac{VD}{v}} \tag{2.11}$$

Where, V is average fluid velocity, D is hydraulic diameter and $\boldsymbol{v}$ is kinematic viscosity that is dependent on temperature. Moreover, the hydraulic diameter for rectangular cooling duct can be calculated by equation 2.12, Table 2.3 shows the hydraulic diameter for each cooling duct width.

$$\boldsymbol{D = \frac{2ab}{a + b}} \tag{2.12}$$

Where ‘a’ is the height of conduit, and ‘b’ is the width of the conduit. Besides, Table 2.3 also shows the Reynolds number for each width in different flow rate. As ‘a’ results, the study models were turbulent.'

Table 2.3 The Reynolds number for each cooling duct width at different flow rate

Width (mm)	Hydraulic Diameter	Reynolds number			
		Flow rate (Litres/min.)			
		4	6	8	10
5	5.00E-03	14050.73	21076.10	28101.46	35126.83
10	6.67E-03	9367.15	14050.73	18734.31	23417.89
15	7.50E-03	7025.37	10538.05	14050.73	17563.42

In reality, when the fluid flows through a pipe, it always has an energy lost against the tube wall. Thus, it causes the pressure to decreases slightly. This phenomenon in pipes is called pressure drop. It can be defined by an energy equation as per below for steady incompressible flows. It was shown by equation 2.13.

$$\frac{\boldsymbol{P_1}}{\boldsymbol{\gamma}} + \boldsymbol{\alpha}\frac{\boldsymbol{V_1^2}}{\boldsymbol{2g}} + \boldsymbol{Z_1} = \frac{\boldsymbol{P_2}}{\boldsymbol{\gamma}} + \boldsymbol{\alpha}\frac{\boldsymbol{V_2^2}}{\boldsymbol{2g}} + \boldsymbol{Z_2} + \boldsymbol{h_L} \tag{2.13}$$

Where, P is the pressure in any section, α is kinetic energy coefficients, γ is specific weight, g is the gravity, Z is level of height and h_L is total head loss [31].

CHAPTER 3

RESEARCH METHODOLOGY

A methodology shows the sequence of the study into 4 sections; pre-modelling, modelling, problem investigating, and the results interpreting. Also, the overall image of the methodology is shown in Figure 3.1, and the description of each section shall be described below.

First of all the pre-modelling, is an awareness of the motor issue in the present. Then, the problem shall be identified what is the real cause of the thermal failure, for specifying the problem. In the specification step, every detail of the induction motor shall be clarified such as a material, the components shape, the assembling method and the principle of rotating. As a result, the best study method, and investigation topic can be selected. Next sequence is a modelling section. The study model shall be created according to the information in the pre-modelling section. This step, the digital mock-up shall be designed following the study topic. There are three investigating topics; the cooling duct width variation (5mm to 15 mm), the cooling duct base diameter variation (270mm to 290mm) and the cooling duct pitch length variation (15mm to 30mm). Hence, eight files of mock-up, and thirty-two analysis cases are created for the thermal invention. Then, the flowchart will move the problem investigating step, it was the computing step. Finally, thirty-two analysis results were interpreted to the report summary.

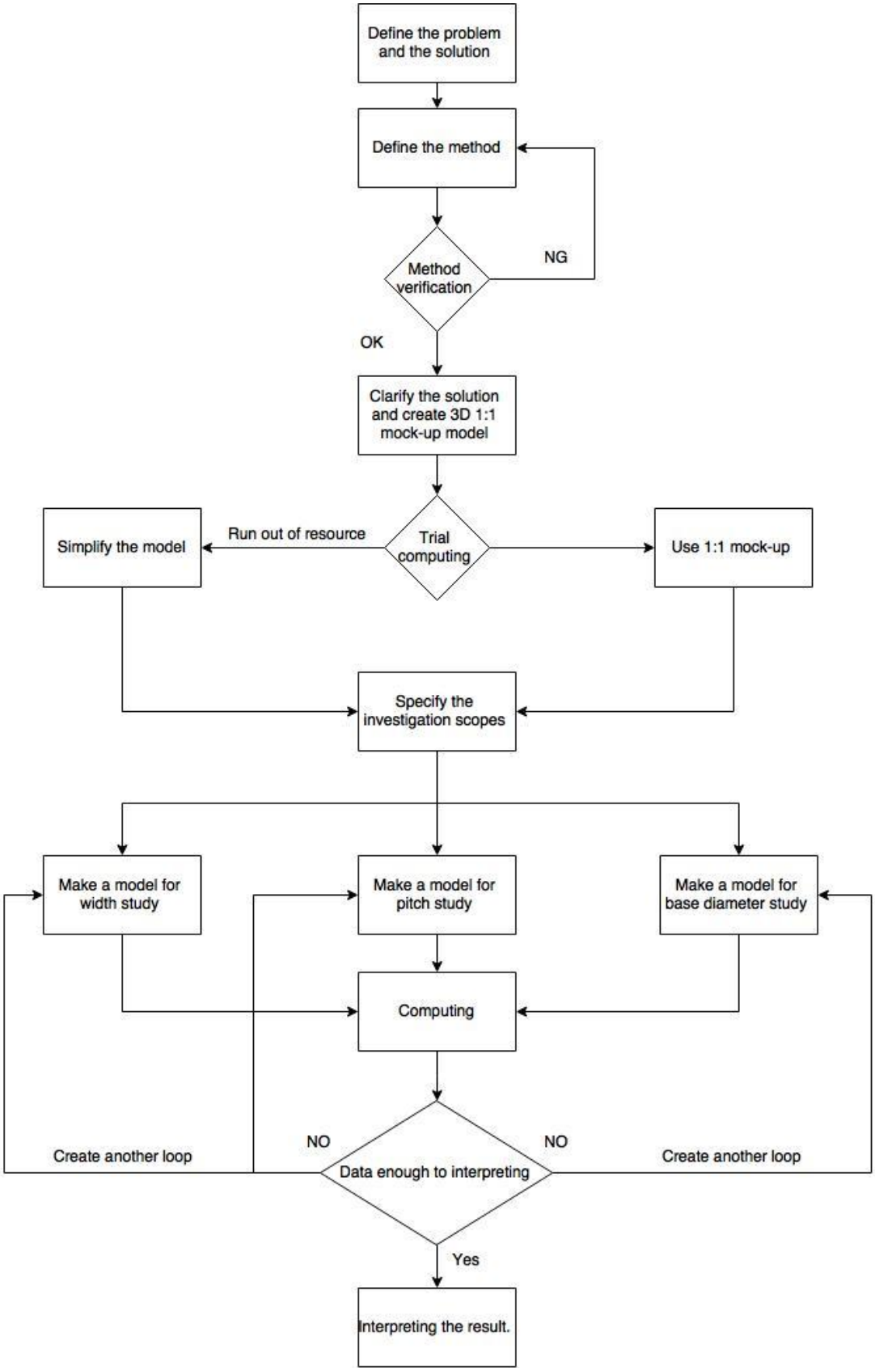

Figure 3.1 Flow Chart for investigation

3.1 Problem specification

The digital mock-up for doing the investigation should be created based on the real item. The main components for mock-up consist of; Stator Body, Stator Laminate, Stator Winding, Rotor Bar and Rotor Core (Rotor).

A stator body is made from steel or aluminium die casting, the inner of the body must be a smooth surface for shrink fitting. The mock-up of stator body can be created by CATIA V5 as shown in Figure 3.2 (left), by using the preliminary information in Appendix A and the real object in Figure 3.2 (right). Similarly, the stator cooling fin is part of the housing, the cooling path shall be grooving on the surface of the stator.

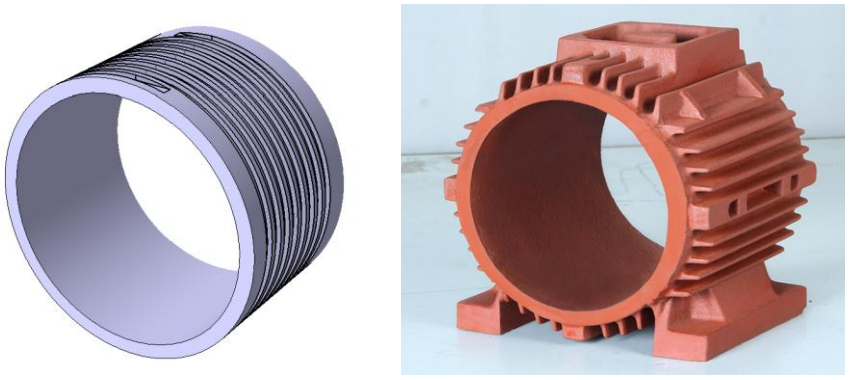

Figure 3.2 (Left) The mock-up of stator body, (Right) The actual of stator body

Stator laminate (Figure 3.3; left) is composed of a layer of steel lamina (Figure 3.3; right) for minimum eddy current losses. The material of the lamina is a high-grade silicon steel/ iron for reducing the hysteresis losses. The stator laminate for a mock-up shall be simplified from a complex shape to a simple shape as shown in Figure 3.4. For example, the outer surface profile shall be changed to a complete circle profile, and the slot quantity shall be reduced from three slots per electricity phase to one slot per phase. As a result, the laminate shall have a complete surface and 36 slots for winding.

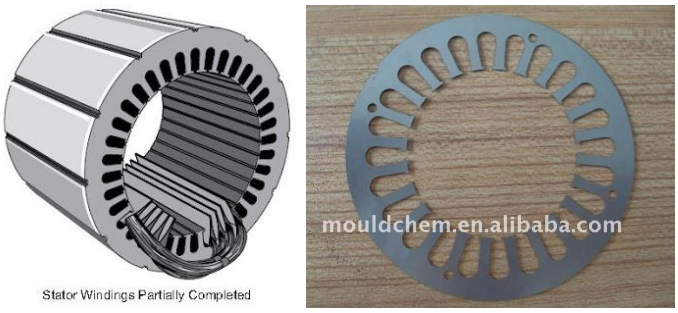

Figure 3.3 (Left) A stator laminate, (Right) A stator lamina

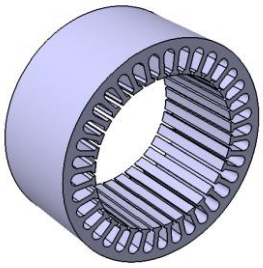

Figure 3.4 A mock-up model of the stator laminate

In general, the stator winding is made from a bundle of copper wire (Figure 3.5). The wire bundle shall carry an electrical current. Therefore, the size of the bundle should be big enough to carry among of the current. However in recent design, the bundle is replaced by a single big wire as shown in Figure 3.6.

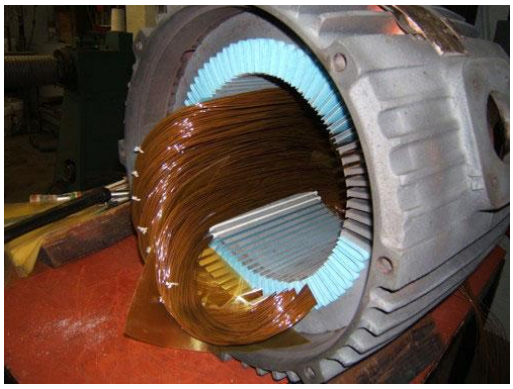

Figure 3.5 A bundle of copper wire (Stator winding)

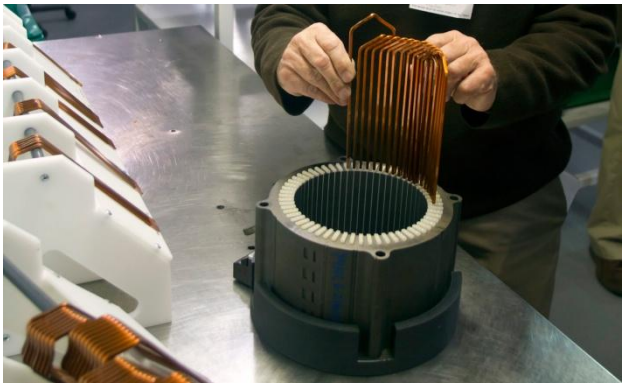

Figure 3.6 A single big wire (Stator winding) [32]

Also, the bundle of copper wire and the single wire are still doing the same function as it were designed; carry the current and induce the magnetic field. Many motors are designed to have 2 or 3 layers of the bundle in the same slot for maintaining the density of magnetic field. Therefore, each bundle must be separated from another. In general, it is separated by a thin film insulator that made from a resin. The bundle mock-up (Figure 3.7) shall be simplified to minimize a computer resource, so the single big wire shall be used a master model for creating in CATIA V5.

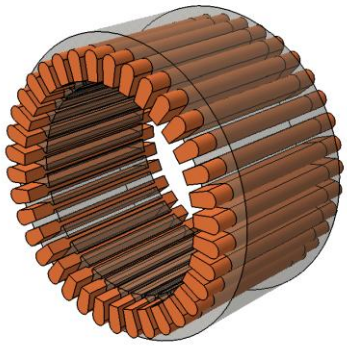

Figure 3.7 A simplified digital mock-up of winding

In general, the stator body and the stator laminate are assembled by shrink fitting method, so these two surfaces shall contact as an imperfect condition. Normally, the thermal contact conductance between aluminium and the steel is 8300 W/m^2 ℃. As well as, a copper bundle shall be inserted into the laminate slot,

and the bundle shall be isolated from contacting to the laminate by a thin layer of insulation material. For example, a glass sheet, a paper.

Furthermore, the rotor consists of three main part; a shaft, a core, and a conductor wire (rotor bar). The rotor core is manufactured same process as stator laminate do. The core shall have a cut out at the outer region for a rotor bar to insert, and the centre of the core shall have a hole for a rotor shaft. The material of a shaft, core and bar are steel, high-grade silicon steel/ iron, and copper/ aluminium respectively. The 3D model shall be simplified for the same reason as the stator and the laminate do. The rotor shaft and the rotor core shall combine to one part, and assume it as a steel material. The rotor bar is assumed to be a copper bar. The end portion of each bar in rotor slot shall be connected by the end ring for the eddy current in the rotor conductor.

Figure 3.8 (Left) A squirrel cage (Right) An iron lamina [26]

In summary, the materials of each part are shown in Table 3.1, and the motor losses in Table 3.2. Moreover, the problem specification can be inferred that it applying the problem specification will help a researcher to prioritize the problem, and it also gives a clearly understand how to make the digital mock-up.

Table 3.1 The material of the motor component

Component	Material
Stator Jacket	Aluminium
Stator Body	Aluminium
Stator Laminate	Steel
Stator winding	Copper
Rotor Bar	Copper
Rotor Shaft	Steel
Rotor Core	Steel

Table 3.2 Energy losses in the motor [33]

Losses Region	Definition	Percents of total losses	Loss at the peak rate (40% of peak power)	
			Verified Model (4kW)	Study Model (80kW)
rotor bar	losses in the rotor conductive	25%	400	8000
stator winding	Heating due to current flow	40%	640	12800
stator teeth	Core losses	10%	160	3200
stator yoke	Leakage fluxes	20%	320	6400
rotor teeth (middle)	Core losses	5%	80	1600
Total		100%	1600	32000

3.2 Three dimension Modelling by CATIA V5

Regarding the preliminary dimension in Appendix A, showing the size of each primary component of the motor, which consists of 1). Rotor; squirrel-cage outer diameter, the cage thickness and Rotor shaft diameter are 180, 120 and 25 mm respectively. 2). Stator Laminated outer diameter, inner diameter and Laminate thickness are 260, 183 and 120 mm respectively. 3). Overall frame outer diameter, inner diameter and the frame total length are 300, 260 and 250 mm respectively. It can be inferred that the clearance between stator and rotor (air gap) is 1.5 mm. The 3D mock-up is shown in Figure 3.9.

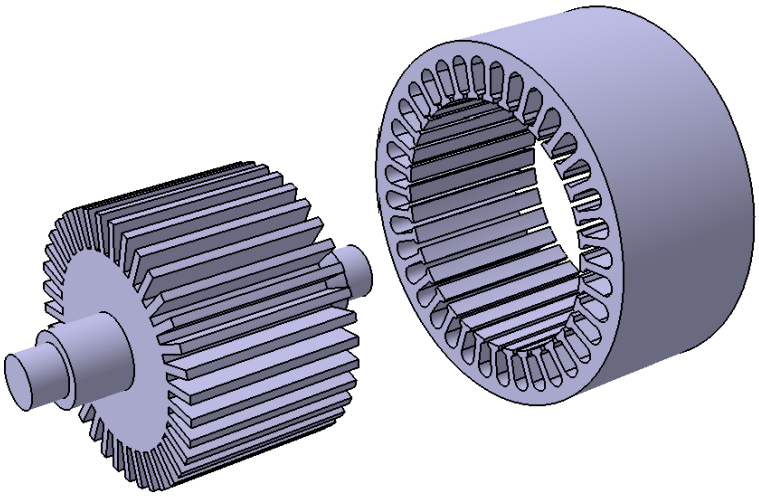

Figure 3.9 The preliminary model. (Left: Rotor, Right: Stator Laminate)

For more understand the propose of investigation, Figure 3.10 illustrates the definition of the cooling duct width, cooling duct base diameter and the cooling duct pitch length. The width study varies the width length from 5mm to 15 mm. The base diameter study varies the diameter from 270mm to 290mm. The pitch length variation the length is from 15mm to 30mm.

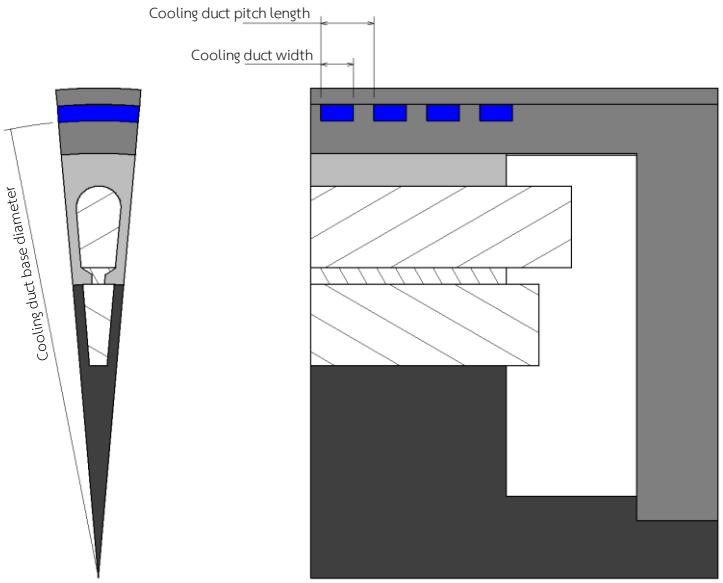

Figure 3.10 A simplified model that show the investigation concern

3.3 Method Verification

The purpose of this studied was not the technique improvement, but it was the applying the essential information from other studies. However, some unclear information made it questionable. Therefore, all applied information should be verified before it was picked to the study model. By comparing several research studies, they have similar information, and it can be concluded as shown in Table 3.2.

The verification shall do the temperature prediction follow “analysis of 3D static temperature field of water cooling induction motor in a mini electric vehicle” [15]. The verification used ANSYS CFX to predict the temperature, and CFX also used 3D mock-up that look similar to the master. The length and the other dimension extracted from the studied results. The key dimensions are as follows;

1) 4kW induction motor cooled by water.

2) Stator laminate contains 30 slots, and the rotor core contains 26 slots.

3) Overall diameter is 200mm.

4) Laminate core and rotor core have 90mm long.

5) Stator laminate outer diameter is 170mm.

6) Rotor diameter is 100mm.

7) Rotor conductor has 20mm high.

8) The height of stator wedge and stator winding are 3mm and 12mm respectively

9) The stator body has 10mm thick.

10) The jacket housing and the cooling path depth have the same thickness that is 5mm.

ANSYS CFX was used to do a temperature analysis, and it was assigned the heat source at the difference location that shown in Table 3.2. Also, the results were extracted in the same pattern with the original studied. The first result is the temperature rise in the radius direction (Figure 3.11), and the other is the temperature contour plot on the object surface (Figure 3.13).

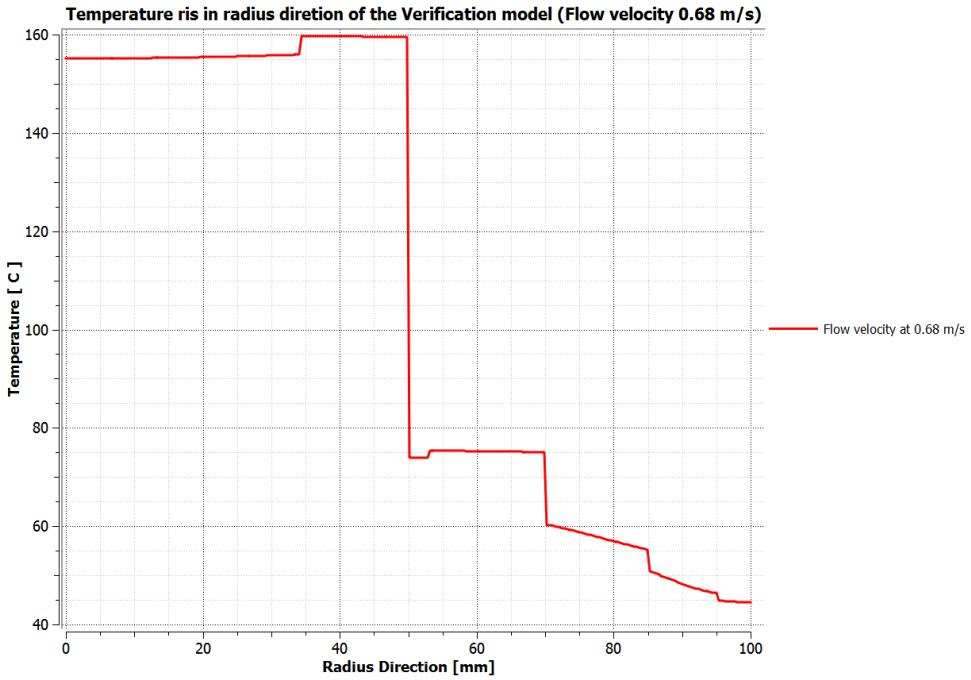

Figure 3.11 The temperature rise in the radius direction of verified model

The Figure 3.11 shows the temperature rise in the radius direction. The horizontal line shows the radius direction from the centre line of the rotor shaft (0mm) to the outer surface of the jacket (100mm). The vertical line shows the temperature in degrees Celsius. The result shows that the temperature at 0mm is 155℃, and it rise to about 157℃ at the lower surface of the rotor bar (34mm). In rotor bar region, the temperature reaches a peak to 160℃ at 34.2mm to 50mm. After that, in the air gap region the temperature slump from the peak to around 73℃. However, at the inner edge of winding region (53mm) the temperature rise to 75℃ until the outer edge of winding. Eventually, the temperature was reduced to 45℃ at the end of jacket housing (r = 100 mm).

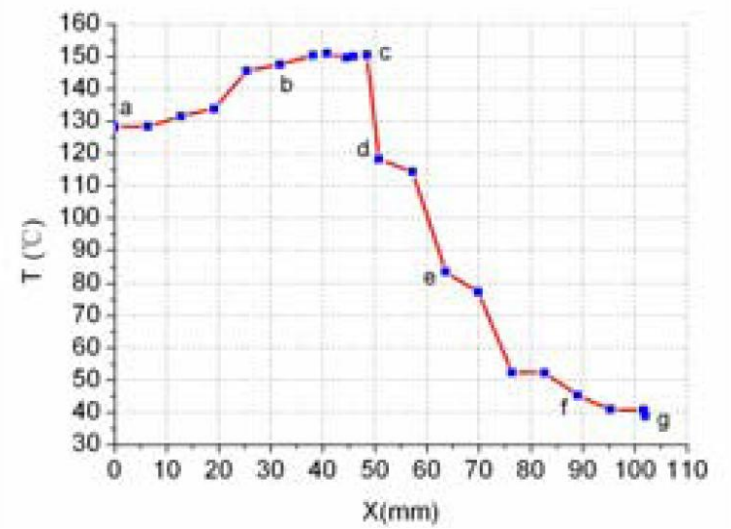

Figure 3.12 The temperature rise in the radius direction of the original model

The Figure 3.12 represents the original result. The core temperature rises to 130°C, and climbs to 148°C at the lower surface of the rotor bar. The temperature still grows until 150°C at the upper surface of the bar. The temperature drops to 115°C at the end of the wedge, and it still falls to 84°C at the top of stator winding. Finally, the temperature in the jacket housing stabilises at 40°C.

When comparing the average temperature in the winding of both graphs (Figure 3.11, and Figure 3.12), the temperature from the validation model is lower than the original model. There are differences in percentage around 25%. However, in the rotor bar region the temperature in the validation is higher than the original around 10°C. Also the other different point is the wedge region; in the original results the temperature is greater than the validation results, and it significant. There are three main factors that make it happen are the material of the wedge, and the wedge in original seems like to be one of the heat sources. Additionally, the other main factor is the heat input or heat source, due to the unknown location and the quantity are made it difference assumption. The verification use 40% of the rate power, it might be over than the original assign to their model. As be shown in the figure, the original model has higher heat transfer ability and/or has the higher heat input than the validation model. Unfortunately, the material of this component is not published,

and it depends on the manufacturer knowledge. Therefore, if the wedge in the validation model has higher heat transfer ability that this, it will raise the temperature in the winding region, and it also reduce the temperature in the rotor region.

Next result is the temperature contour plot on the object surface. The contour plot shows the temperature from the lowest to the highest. Both Figure 3.11 and Figure 3.13 show the maximum temperature at the outer surface of the rotor bar, and the minimum temperature at the water region.

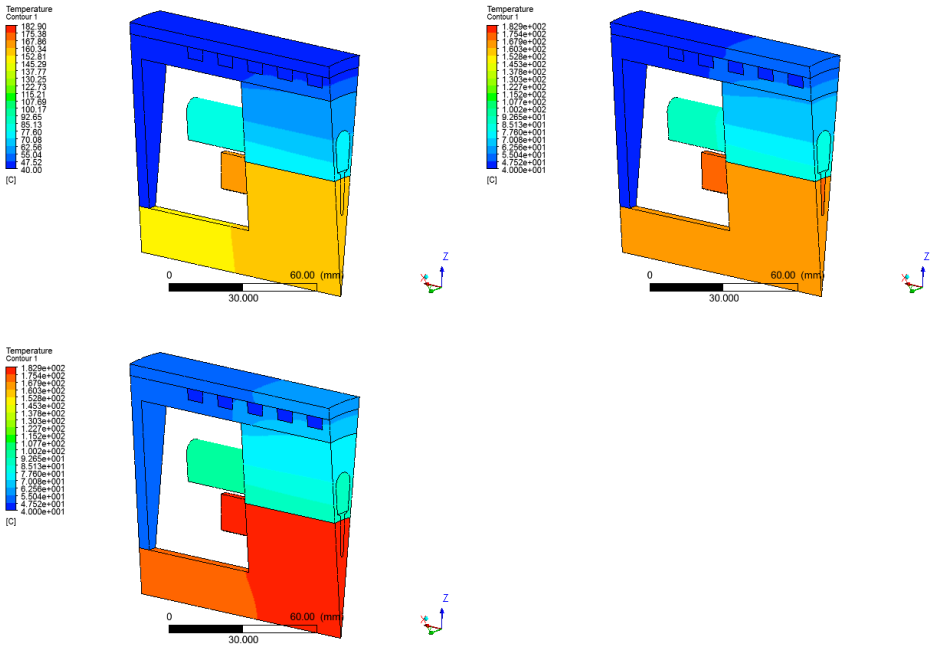

Figure 3.13 A temperature contour port at the surface of the verified model

CHAPTER 4
FINITE ELEMENT ANALYSIS RESULTS AND DISCUSSIONS

From the temperature curve shown in Figure 3.11, the trend does not give any valuable information to be interpreted. Therefore, more data will be used to explain in this chapter which consists of three sections. First is about the maximum temperature. Next is the temperature contour plot on the surface of the motor and the temperature in the middle section of the simplified model. Finally, the behaviour of heat flux will be described.

4.1 Analysis Results

Table 4.1, Table 4.2, and Table 4.3 show the temperature for each study model. Each letter in a model is described as; P-Pitch length, W-Channel Width, and B-Base diameter. For example, P20W10B270 denotes 20 mm pitch, 10 mm width, and 270 mm base diameter. These tables show the maximum global temperature in each component. The highest temperature or motor hot spot is in the Rotor bar region. However, the biggest failure factor of induction motor contributes to the short circuit at the end winding. Only a few occur in the rotor bar because of the thermal stress[11]. Therefore, the maximum temperature shall be focused on the winding and rotor bar temperature. Additionally, this motor was cooled by water via a cooling pump. Therefore, the pressure drop should be considered as well.

Table 4.1 Maximum temperatures in different components (varied by width)

Model	Location	Maximum Temperature (Unit: °C)			
		4 L/min	6 L/min	8 L/min	10 L/min
P20W05	Maximum Temperature	162.208	160.627	159.072	155.988
	Winding	101.383	100.623	100.25	99.974
	Bar	162.208	160.627	159.072	155.988
	Laminate	78.198	77.438	77.063	76.779
	Rotor	153.047	151.473	149.927	146.864
	Pressure drop (kPa)	187.584	420.736	713.408	1056.064
P20W10	Maximum Temperature	151.494	151.415	149.828	149.807
	Winding	102.102	100.775	100.074	99.704
	Bar	151.494	151.415	149.828	149.807
	Laminate	78.885	77.563	76.863	76.494
	Rotor	142.419	142.33	140.751	140.727
	Pressure drop (kPa)	30.464	74.432	137.984	218.176
P20W15	Maximum Temperature	143.798	142.139	142.089	142.057
	Winding	103.156	101.262	100.319	99.748
	Bar	143.798	142.139	142.089	142.057
	Laminate	79.934	78.04	77.098	76.528
	Rotor	134.79	133.13	133.073	133.038
	Pressure drop (kPa)	10.752	26.496	50.24	81.984

Furthermore, the value in Table 4.1 can be used to plot the temperature trend in winding, Bar and pressure drop as shown in Figure 4.1, Figure 4.2 and Figure 4.3.

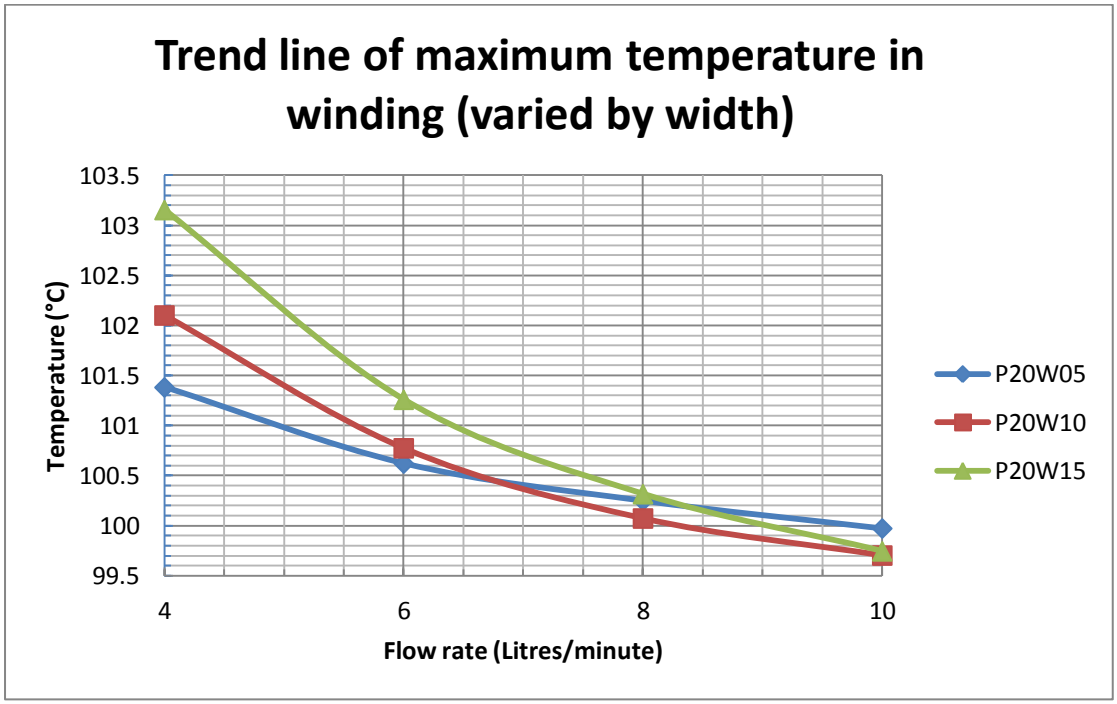

Figure 4.1 Trend line of maximum temperature in winding (varied by width)

shows curves of maximum temperature trend in the stator winding. The curves display relationship between maximum temperature and water flow rate. Each line represents different channel width model. The Blue, Red, and Green show the channel width of 5 mm, 10 mm, and 15 mm respectively. The curves show that temperature gradually reduced when flow rate increased. From Table 4.1, the highest temperature is 103.156℃ at 4 L/min from 15 mm width model, and the lowest is 99.748℃ at 10 L/min from the same model. However, considering the specific flow rate such as 10 L/min and vary only the channel width, the temperature is similar at around 99℃. Additionally, to see the relationship between temperature and flow rate, 5 mm, and 15 mm model were selected for consideration. At 5 mm width, the temperature between 4 L/min and 10 L/min has the difference around 1.7℃. When consider 15 mm model, the change is around 3.4℃. However, this cannot be clearly assumed that the flow rate has an influence on the temperature changing.

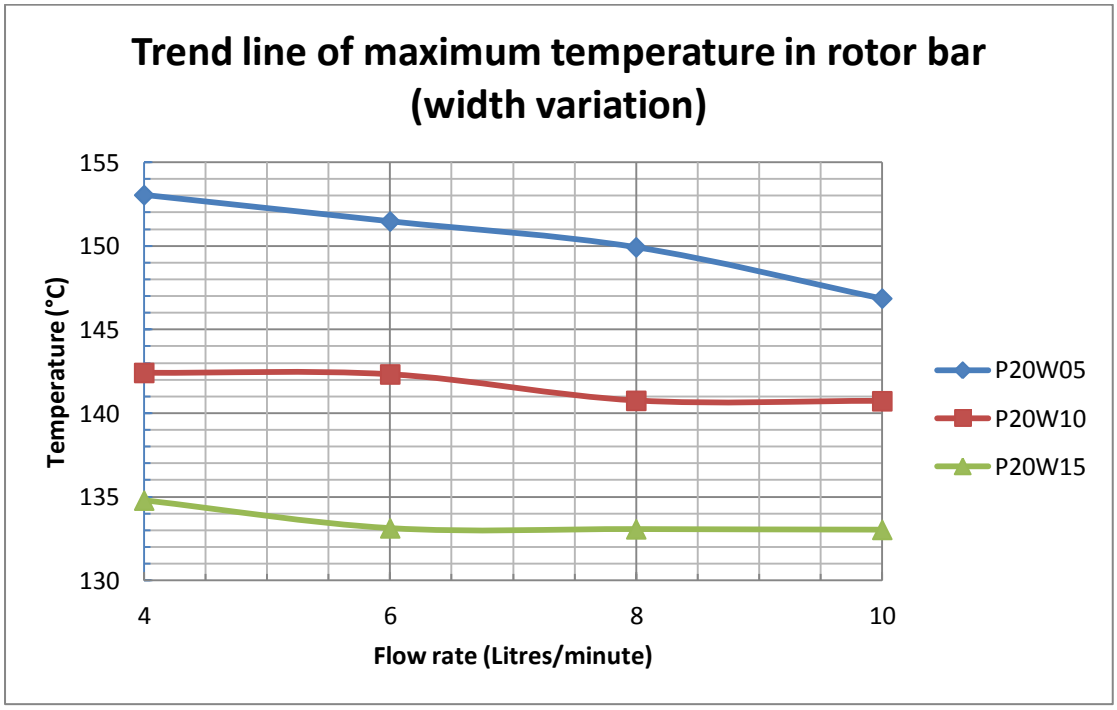

Figure 4.2 The trending line of maximum temperature in rotor bar (width variation)

On the other hand, the maximum in Bar of 5mm is 162.208℃ when the flow rate is 4L/min, but when it is changed to 10L/min the temperature was reduced to 155.988℃ or which decreased by 6.2℃. Additionally, 15mm width produced 143.798℃ and 142.057℃ which decreased by 1.7℃ when flow rate changes from 4 to 10 litres per minute. When consider flow rate at 4L/min, 15 mm model produces lower temperature than 5 mm by 18.4℃. At 10L/min, temperature is also lower than 5 mm by 13.931℃.

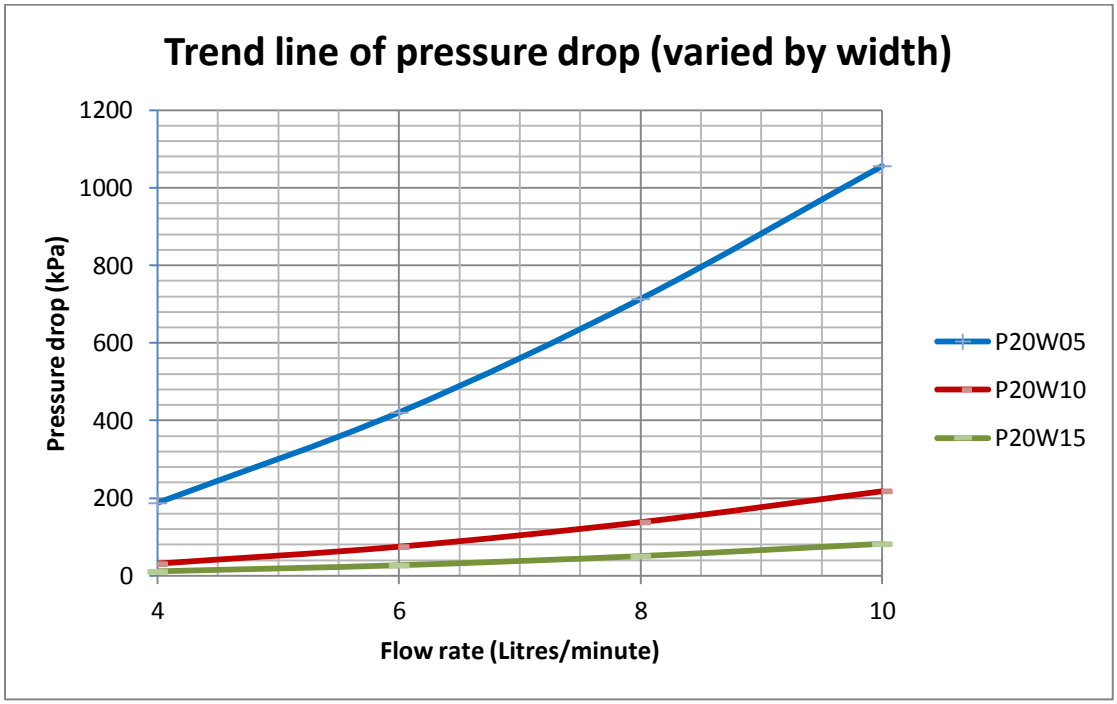

Figure 4.3 Trend line of pressure drop (varied by width)

Moreover, the pressure drop trend can be plotted as shown in Figure 4.3. This displays the behaviour of pressure drop when flow rate is changed. At 5 mm channel width, the pressure drop is a dramatically increased. However at 10 mm and 15 mm, pressure drop is gradually increased. The reason that 5 mm stands out from the other curves because the 5 mm have a hydraulic diameter smaller two times smaller than 10 mm and three times smaller than 15 mm. Hydraulic diameter is the factor which directly related to the water velocity. This is the main cause that raise the pressure drop in every pipe. Figure 4.3 shows that the initial pressure is at 187.584 kPa for 5 mm width and is increased to 1053.064 kPa. The curves also show that the pressure drop of 10 and 15 mm model is 30.464 kPa and 10.752 kPa respectively, and the pressure drop in these two models rise to 218.176 kPa and 81.984 kPa respectively. In the graph, it can be inferred that the 5 mm width is not suitable for this motor because it consumes much more power for pumping circulation water.

However, the value in Table 4.1 is a maximum temperature which cannot show temperature contour plot on the surface for displaying the location or locate the

distribution. Figure 4.4 and Figure 4.5 show the temperature distribution in the middle section and the surface of the simplified model.

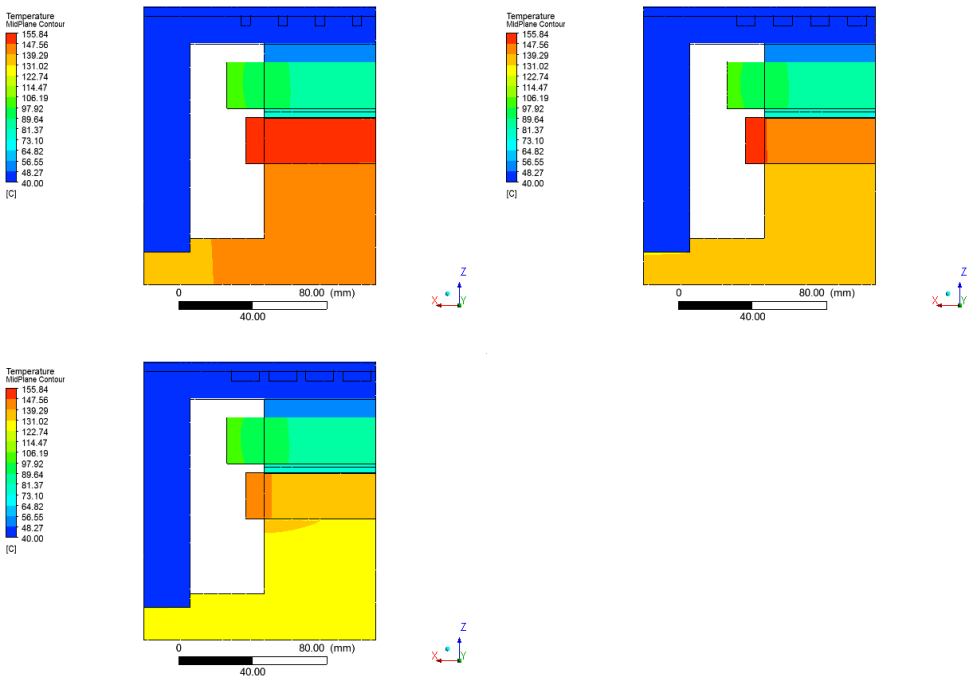

Figure 4.4 Temperature distribution from the middle section of the studied model (Top Left: 5mm, Top Right: 10mm and Lower Left: 15mm)

It can be seen that the highest temperature zone is located at the rotor region especially near the rotor conductor. The high temperature is spread to the centre of the rotor ("-Z" direction) and also spread to the front side of the rotor. It is clearly seen in 5mm channel width model that the energy is transferred from the rotor conductor to the centre line, and it has potential to move to stator body. Unfortunately, the interface between the rotor and the stator body was assigned as bearing given the 2 mm of air in contact. On the other side, the stator winding is also given the energy to the laminated stator which then transferred to the stator body for releasing to cooling fluid. Figure 4.4 and Figure 4.5 show comparison among of the width study.

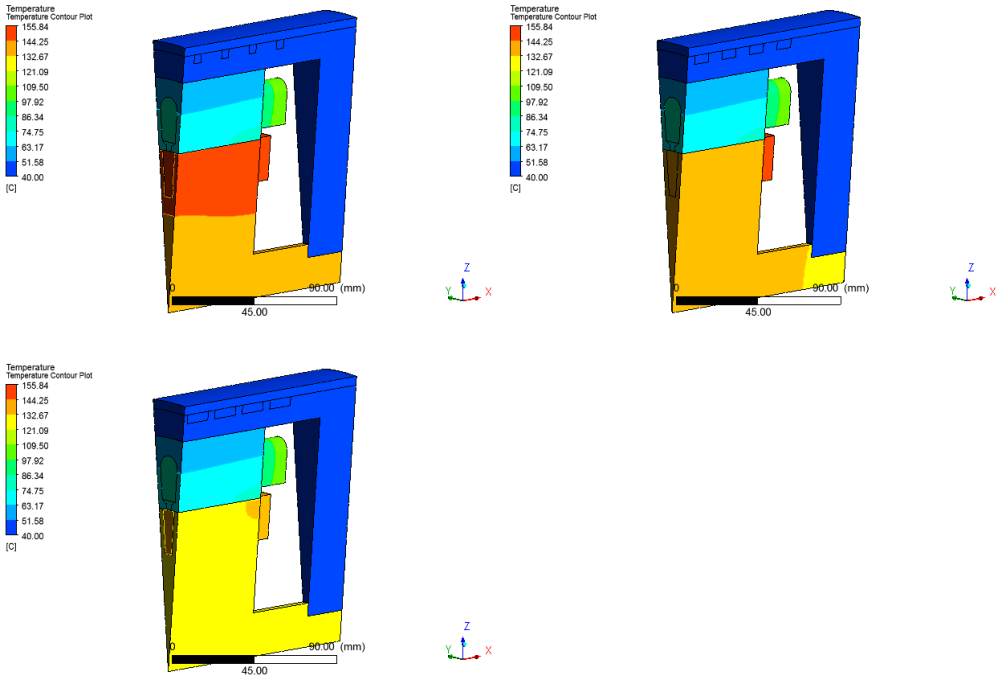

Figure 4.5 Temperature distribution at the surface of the studied model
(Top Left: 5mm, Top Right: 10mm and Lower Left: 15mm)

In addition, the base diameter variation, the maximum temperature and the pressure drop in each component are shown in Table 4.2. The difference of temperature between 4 L/min and 10 L/min in 270mm diameter is 2.65℃, and for 290mm is 2.18℃. Also, the rotor bar with 270mm and 290mm has temperature difference around 3.25℃ and 2.28℃ respectively.

Table 4.2 The maximum temperature in the different components (varied by base diameter)

Model	Location	Maximum Temperature (Unit: °C)			
		4 L/min	6 L/min	8 L/min	10 L/min
P20W10B270	Maximum Temperature	149.821	148.187	148.145	146.574
	Winding	99.959	98.46	97.749	97.301
	Bar	149.821	148.187	148.145	146.574
	Laminate	76.749	75.252	74.543	74.093
	Rotor	140.745	139.113	139.066	137.504
	Pressure drop (kPa)	29.504	72.128	133.952	211.392
P20W10B280	Maximum Temperature	151.494	151.415	149.828	149.807
	Winding	102.102	100.775	100.074	99.704
	Bar	151.494	151.415	149.828	149.807
	Laminate	78.885	77.563	76.863	76.494
	Rotor	142.419	142.33	140.751	140.727
	Pressure drop (kPa)	30.464	74.432	137.984	218.176
P20W10B290	Maximum Temperature	154.708	153.086	153.049	151.481
	Winding	104.119	102.837	102.233	101.84
	Bar	154.708	153.086	153.049	151.481
	Laminate	80.9	79.619	79.018	78.624
	Rotor	145.623	144.004	143.963	142.405
	Pressure drop (kPa)	31.488	76.928	142.656	225.536

Additionally, the pressure drop in each model is similar to each other. The different pressure drop at low flow rate is around 1.98 kPa and 14.14 kPa at high flow rate (10 L/min) as shown in Figure 4.7 From these two factors, it can be inferred that the flow rate has a same effect with base diameter change. Besides, by changing the base diameter close to the centre by 10 mm the temperature can be reduced by 2-3°C as shown in Figure 4.6.

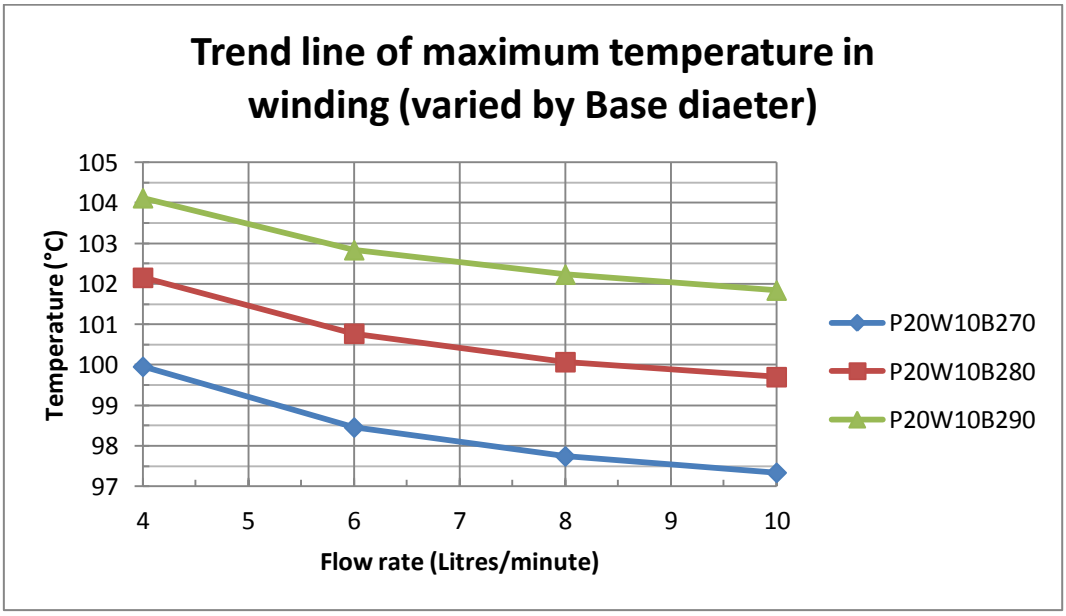

Figure 4.6 Trend lines of maximum temperature in winding (varied by base diameter)

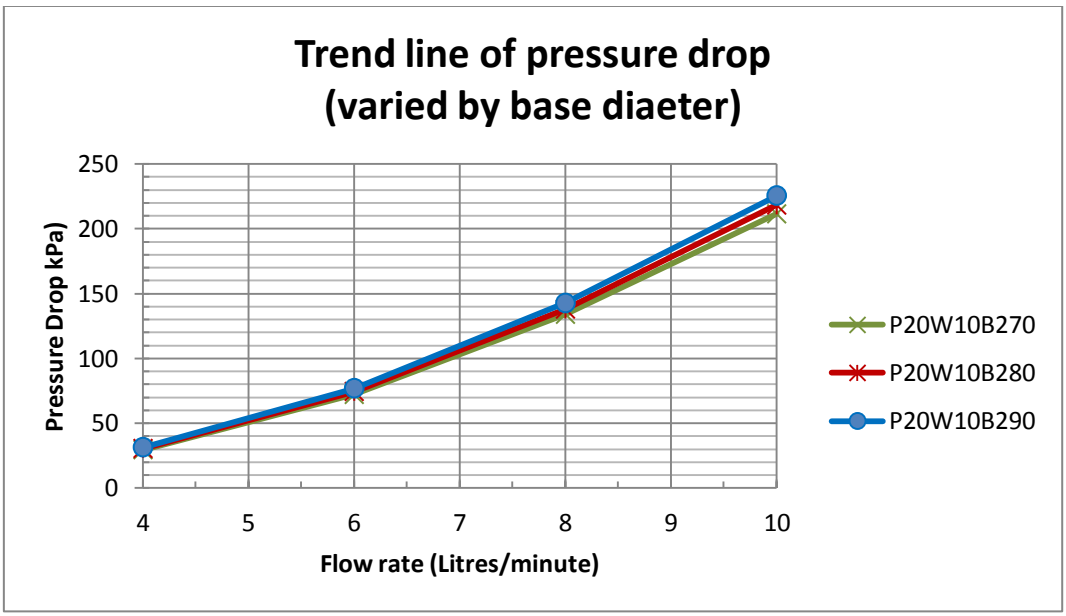

Figure 4.7 Trend line of pressure drop (varied by base diameter)

Moreover, the temperature distribution is shown in Figure 4.8 and Figure 4.9. As a result, this shows same behaviour of the heat transfer to previous data.

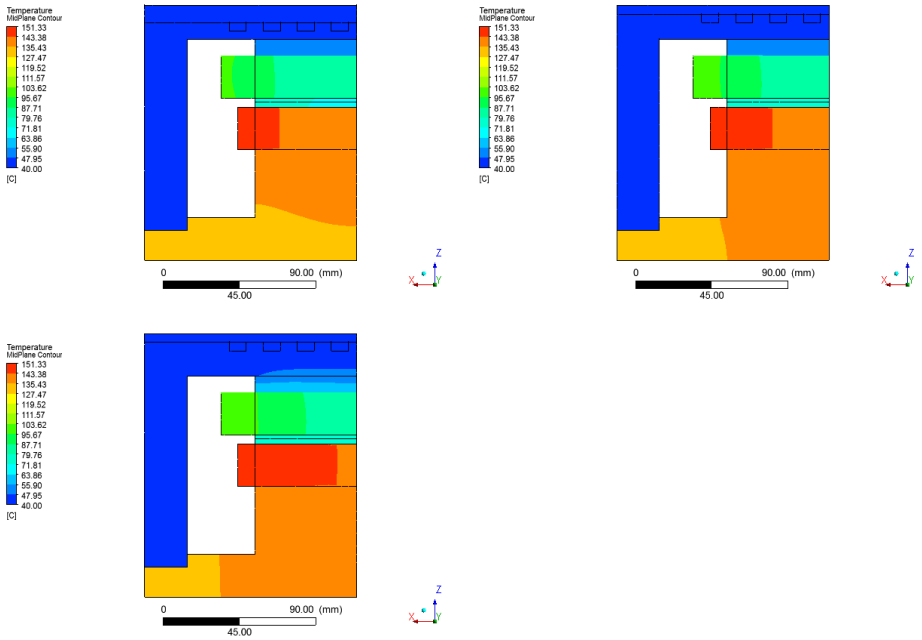

Figure 4.8 Temperature distribution from the middle section of the studied model (Top Left: 270mm, Top Right: 280mm and Lower Left: 290mm)

Figure 4.9 shows the temperature distribution at the surface, it also shows that the temperature does not change so much as variation of width (see Figure 4.5). Therefore, it can be assumed that the width variation has an effect on the temperature in rotor region more than the base diameter variation.

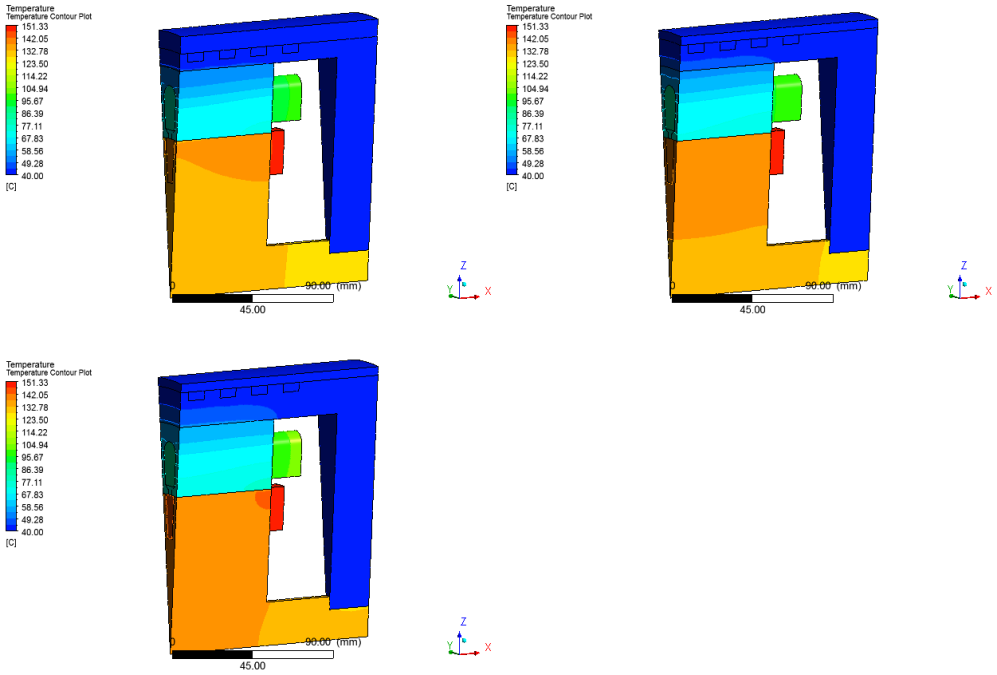

Figure 4.9 Temperature distribution at the surface of the studied model (Top Left: 270mm, Top Right: 280mm and Lower Left: 290mm)

Moreover, the pitch length variation did the same phenomena and the maximum temperature is shown in Table 4.3.

Table 4.3 The maximum temperature in the different components (varied by pitch)

Model	Location	Maximum Temperature (Unit: °C)			
		4 L/min	6 L/min	8 L/min	10 L/min
P15W10	Maximum Temperature	151.494	149.864	149.825	148.255
	Winding	101.85	100.482	99.843	99.431
	Bar	151.494	149.864	149.825	148.255
	Laminate	78.675	77.298	76.655	76.24
	Rotor	142.421	140.794	140.751	139.189
	Pressure drop (kPa)	30.4	74.368	138.048	218.048
P20W10	Maximum Temperature	151.494	151.415	149.828	149.807
	Winding	102.102	100.775	100.074	99.704
	Bar	151.494	151.415	149.828	149.807
	Laminate	78.885	77.563	76.863	76.494
	Rotor	142.419	142.33	140.751	140.727
	Pressure drop (kPa)	30.464	74.432	137.984	218.176
P25W10	Maximum Temperature	153.134	151.487	151.44	149.866
	Winding	103.64	101.95	101.163	100.668
	Bar	153.134	151.487	151.44	149.866
	Laminate	80.397	78.713	77.93	77.436
	Rotor	144.057	142.411	142.359	140.793
	Pressure drop (kPa)	22.848	55.744	103.488	163.52
P30W10	Maximum Temperature	154.737	153.08	151.48	151.451
	Winding	104.712	102.829	101.893	101.395
	Bar	154.737	153.08	151.48	151.451
	Laminate	81.445	79.57	78.637	78.141
	Rotor	145.654	143.997	142.403	142.371
	Pressure drop (kPa)	22.784	55.744	103.424	163.52

The Winding temperatures at 4 L/min are 101.85℃, 102.102℃, 103.64℃, and 104.712℃ for Pitch 15 mm, Pitch 20 mm, Pitch 25 mm, and Pitch 30 mm respectively. It can be seen that the temperature trend increases gradually when pitch length was increased. Besides, pressure is also separated into two groups. The first group has eight loops of cooling duct per motor (15 mm and 20mm) and the second group has six loops (25 mm and 30 mm). At 4 L/min, the pressure drop of eight loops is at 30.4 kPa and was reduced to 22.784 kPa when the loops was changed to six. As a result, when increasing the flow rate to 10 L/min the pressure drop was increased to around 163 kPa and 219 kPa for six loops and eight loops respectively.

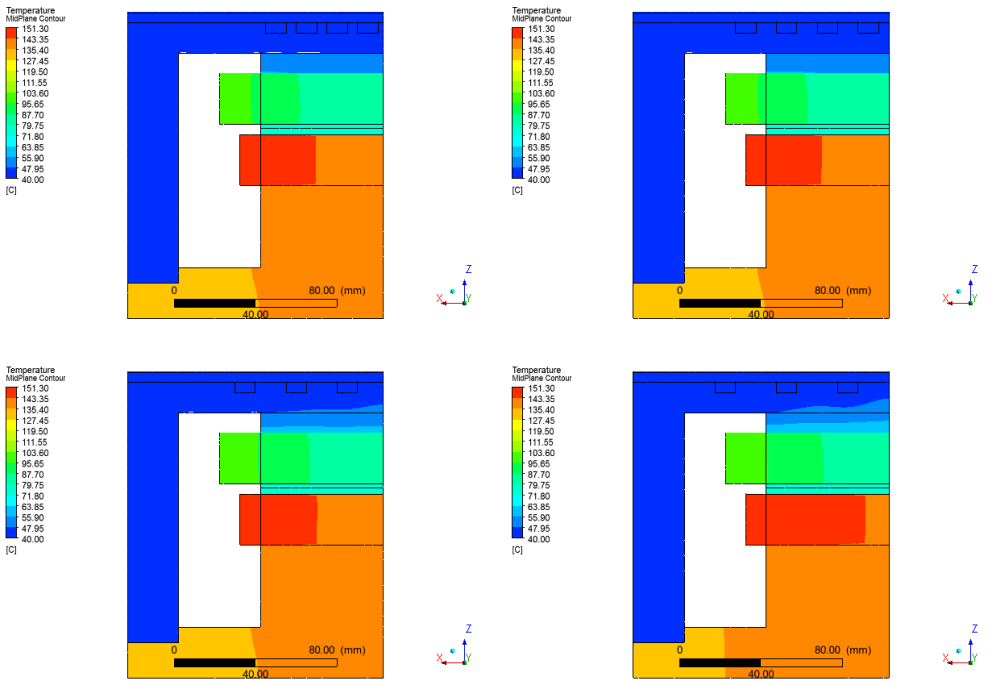

Figure 4.10 Middle plane temperature contour of the studied model
(Upper Left: 15mm, Upper Right: 20mm, Lower Left: 25mm, and Lower Right 30mm)

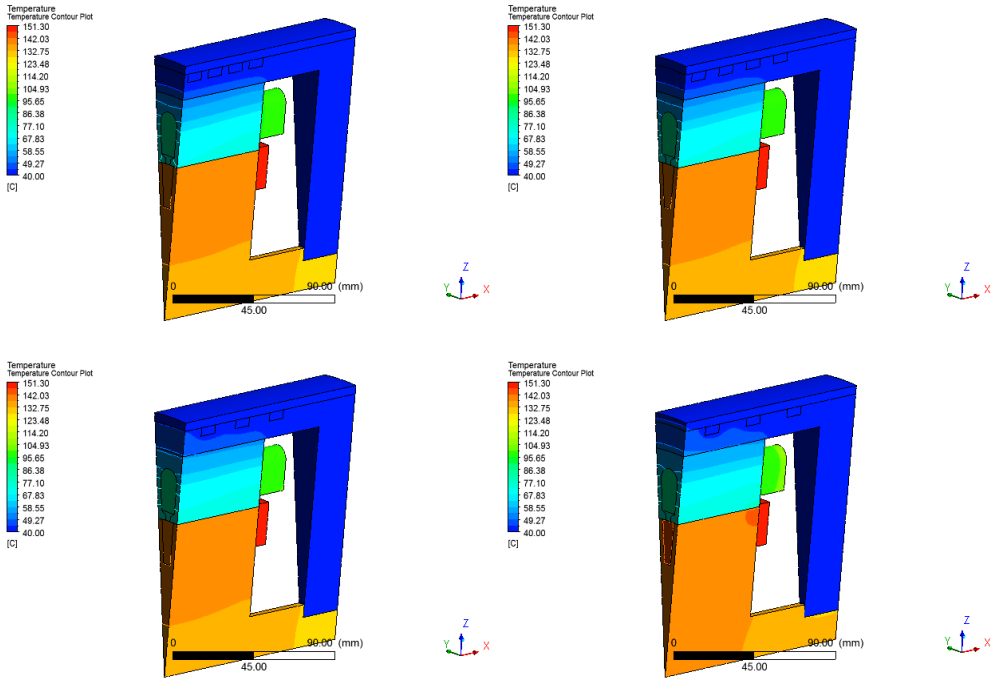

Figure 4.11 Temperature distribution at the surface of the studied model (Upper Left: 15mm, Upper Right: 20mm, Lower Left: 25mm, and Lower Right 30mm)

In summary, the lowest temperature in each study model is from 10 L/min. Firstly the width of the cooling investigation, the temperature is at lowest (80°C) at the 15mm duct width. Secondly from base diameter investigation, the temperature is at lowest from 270mm model (close to the heat source) and highest at 290mm model. Therefore, it can be inferred that if the closer cooling system to the heat source, the waste energy will be removed more efficiently. However, this investigation was done by varying of stator body surface. So, this shall use the same diameter as it was configured in the preliminary design (280mm). Lastly, the pitch length investigation, Table 4.3 shows the same temperature results between 15mm and 20mm model. This means the temperature is related to the covering area of the inlet region. Besides, the selection of the pitch and the width should be related but the 15mm pitch length shall not match with 15mm width. Therefore, in full-scale mock-up, the cooling duct width shall be 10mm with 16.25mm pitch length.

4.1.1 The result of the Full-scale model analysis

The final result was approached by combining results together. The cooling duct profile has 10mm width, 280mm base diameter and 16.25mm pitch length. Here, the same heat source shall be assumed and applied to ANSYS CFX. Figure 4.12 shows the temperature distribution in the lateral plane and Figure 4.13 shows the temperature distribution in the longitudinal plane. Both temperature distributions in the simplified mock-up and the full-scale mock-up produce similar results. The highest temperature is in the rotor region, and the highest of rotor region is closed to the end bar. On the winding, the temperature is also similar. Finally, all of the results have only 75% of reliability by comparing to the existing research literatures.

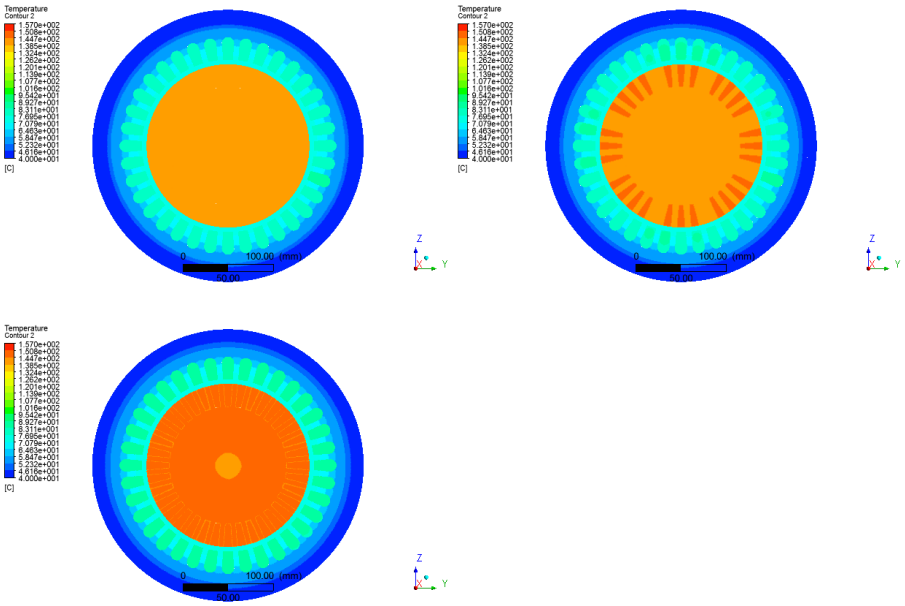

Figure 4.12 The temperature distribution in the lateral plane of the full-scale model (Upper left: 10 L/min, Upper right: 8 L/min and Lower left: 6 L/min)

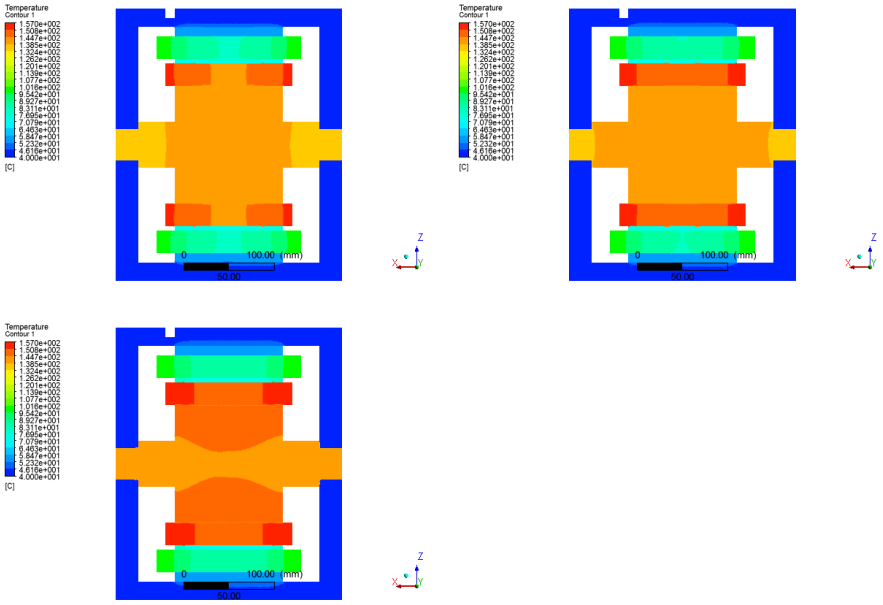

Figure 4.13 The temperature distribution in the longitudinal plane of the full-scale model (Upper left: 10 L/min, Upper right: 8 L/min and Lower left: 6 L/min)

4.2 Results Discussion

To understand the behaviour of the temperature distribution, heat flux shall be selected to analyse. The explanation will start from the main heat source (Stator Winding & Rotor Conductor Bar). Figure 4.14 shows the heat flux of the rotor bar, it can be seen that the range of the indicator shows the plus value to the minus value.

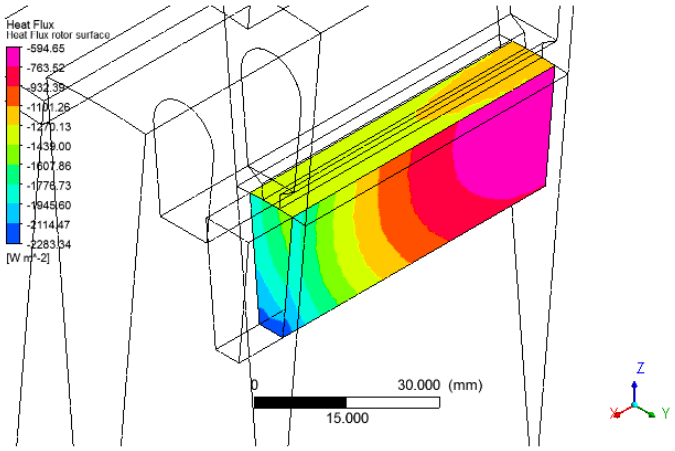

Figure 4.14 Heat Flux in direction out of Rotor Conductor Bar

In general, the heat flux direction is perpendicular to the one as shown in Figure 4.15; line "A" is perpendicular to the curve "B". Therefore, the plus value means that heat flux goes to the inside of the surface in the perpendicular direction. On the other hand, the minus value means that heat flux goes out to the next object. It can be observed that “plus” is “flux in” and “minus” is “flux out”.

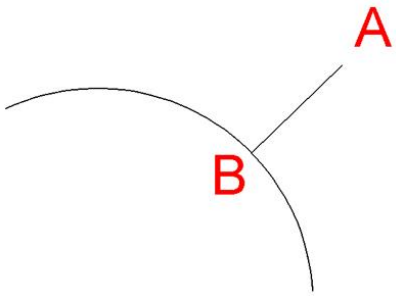

Figure 4.15 The perpendicular line on the curve

Figure 4.14 shows that the “heat flux in” was located in the frontal area or close to the end region only. This means that the “heat flux in” at the end region that did not interface to any surface attempts to transfer the heat to the next component. On the top area, the heat flux moved out to the laminated stator wedge, the density was higher at the frontal area which has the effect to the end region. In the other interface, the rotor core also received the heat flux from the rotor bar. The density was higher in the front area as well.

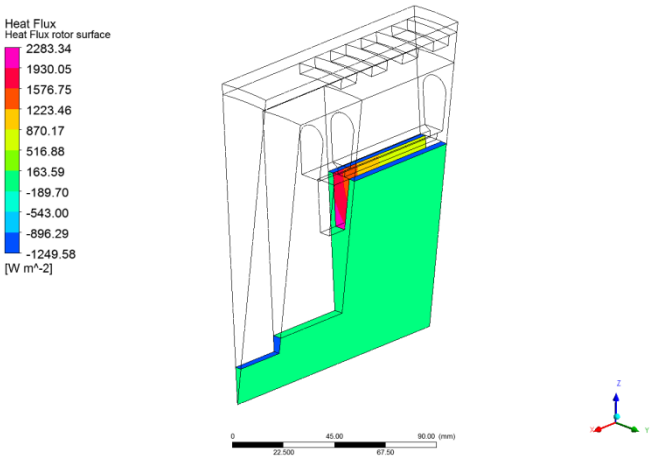

Figure 4.16 Heat Flux of Rotor Region

Figure 4.16 also shows similar indicator; plus & minus values. The “flux in” receives the heat from the interface with the rotor conductor bar, and that heat flux was released into two areas; the body interface and the laminated interface.

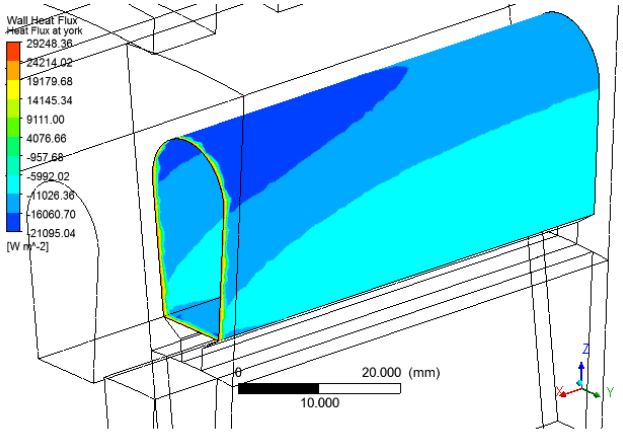

Figure 4.17 Heat Flux of Stator Winding

For the stator side, stator winding was also one of the heat sources. Figure 4.17 shows that the behaviour of the stator winding is the same as rotor bar’s results. The higher density of plus value was in the front area near the end region. The highest density of minus value was on the top-front section of the winding. The reason is that frontal area is close to two cooling channel. The figure also shows the heat flux

that moved out every direction of the winding surface. Thus, transfer the heat to the laminated and the wedge.

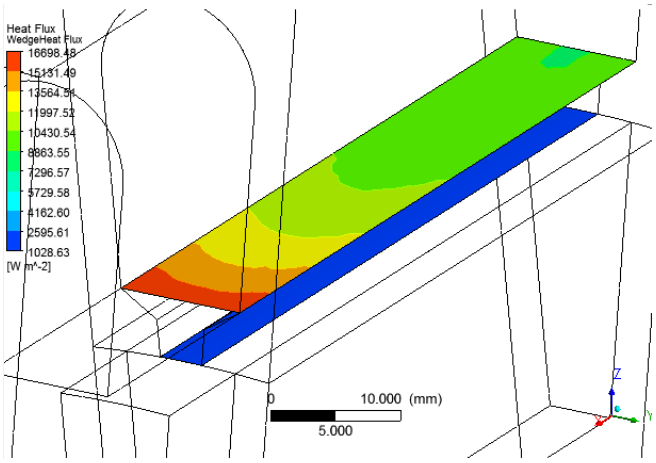

Figure 4.18 Heat Flux in direction to the Stator Wedge (plus value)

To simplify, two figures of the stator wedge will be used for describing “flux in” and “flux out”. Firstly, Figure 4.18 shows that the wedge received heat flux from the stator winding and the rotor bar at the bottom.

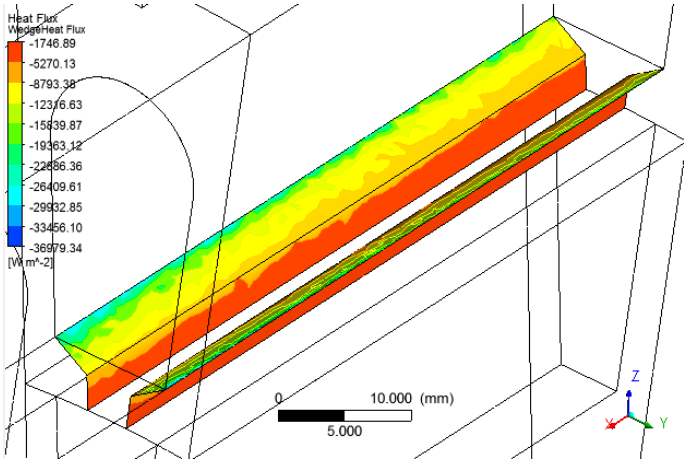

Figure 4.19 Heat Flux in direction out (minus value) of Stator Wedge

Secondly, Figure 4.19 shows the heat “flux out” of the stator wedge. The highest minus density is on the top of the wedge. Therefore, it can be seen that

most of the heat source transferred to the laminated stator only not from direct contact but also from the indirect contact (wedge and rotor).

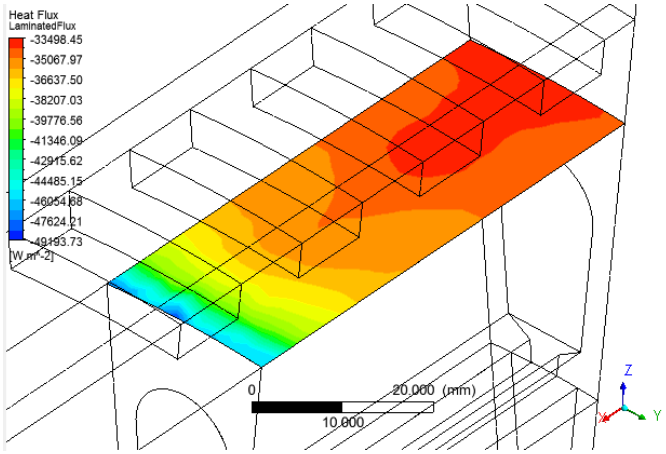

Figure 4.20 Heat Flux in direction out (minus value) of Stator laminated

In the laminated, the minus value had the highest magnitude at the frontal area as same as the winding and the rotor bar and the value was reduced to the middle of the motor as shown in Figure 4.20. Moreover, the heat flux almost dumped to the cooling fluid, but some of heat was still transferred to the jacket as shown in Figure 4.21. Therefore, the jacket had to release the heat back to the stator body at the low temperature or in the front of the stator body that supposed to be the cover. Thus, this is the other reason that make the temperature in the front end of the stator body produce temperature difference.

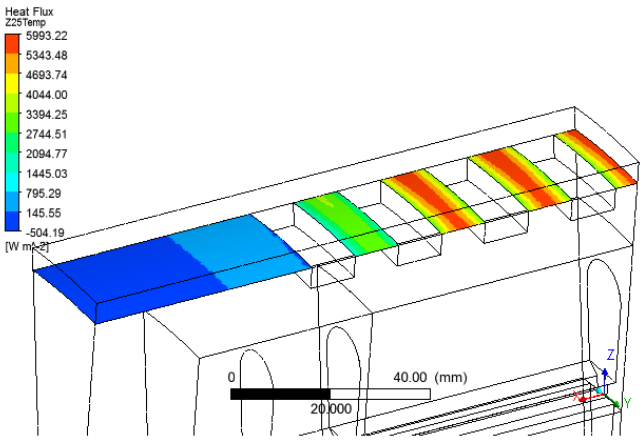

Figure 4.21 Heat Flux in (Blue) and out (Red) of Stator Jacket

As a result, Figure 4.22 shows the temperature at the middle plane of the jacket. It shows that the jacket has the highest temperature between the cooling duct, and it will affect the front side that increased the temperature.

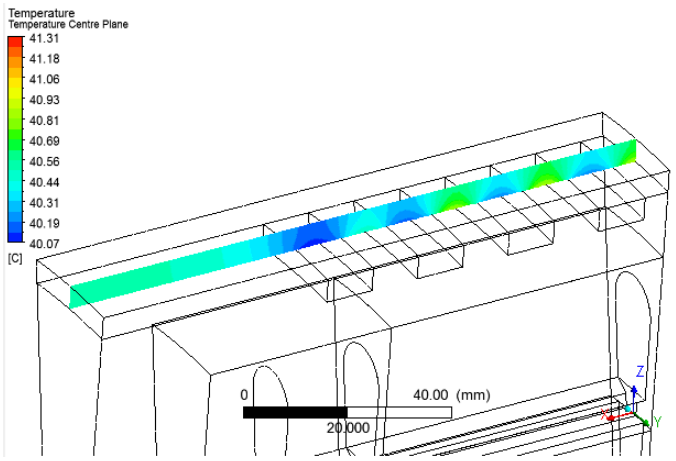

Figure 4.22 Temperature distribution in the middle section of the Stator Jacket

Therefore, including the temperature distribution, Figure 4.23 shows the distribution at the frontal area close to the rotor, as well as the laminated interface. The temperature layer in laminated interface is quite varied because it is closed to the heat flux from the laminated stator.

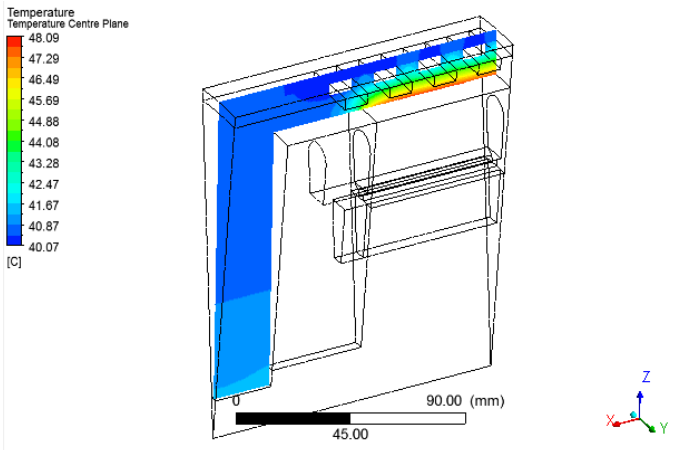

Figure 4.23 Temperature distribution in the middle section of the Stator Jacket and body

Moreover, when changing the indicator scale by adding the laminated surface to the figure, the temperature is quite diverted at the upper of the laminate. Additionally, at the surface itself, the temperature distributed to the lower portion of the laminated is the highest. This was located at the front end of the rotor bar the interface.

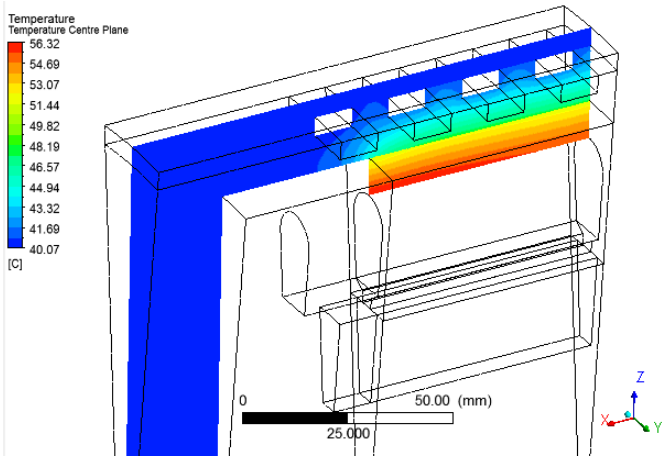

Figure 4.24 Temperature distribution in the middle section of the Stator (Maximum scale at 56.32°C)

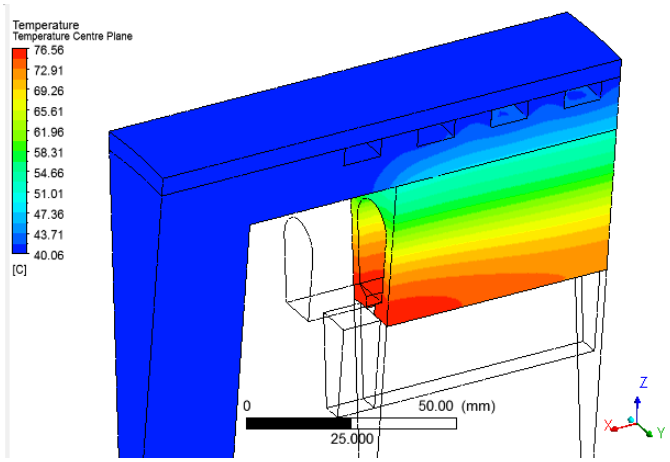

Figure 4.25 Temperature distribution in the surface of the Stator (Maximum scale at 76.56°C)

Additionally, the temperature distribution (see Figure 4.26) in the rotor is also related to the above evidence. The above phenomena explains the cause of the motor failure which almost happen at the end winding and some with the broken rotor conductor bar.

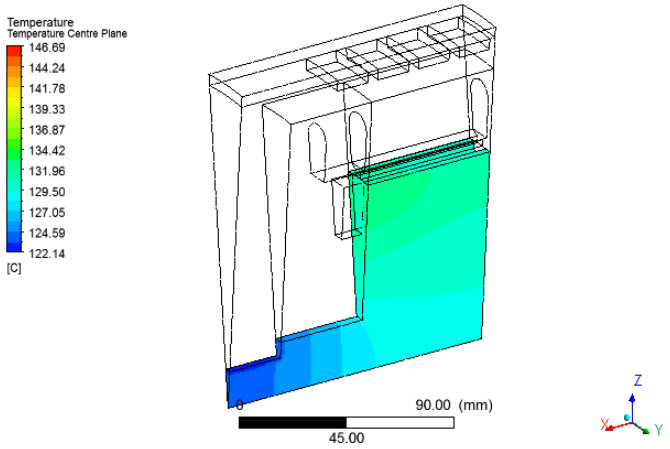

Figure 4.26 Temperature distribution in the surface of the rotor

Moreover, from the channel width variation, there had no relationship between the temperature in the stator and the rotor. Table 4.1 shows that the temperature in the stator winding was still the same when changing the channel width. However, the temperature of rotor region is quite effective to the width variation. To understand this contrast, the previous mechanism can be used to explain. The temperature distribution in Figure 4.26 and the heat flux change in Figure 4.16 can be used to explain the rotor, and the heat flux in Figure 4.14 will be used to describe the rotor bar temperature contrast.

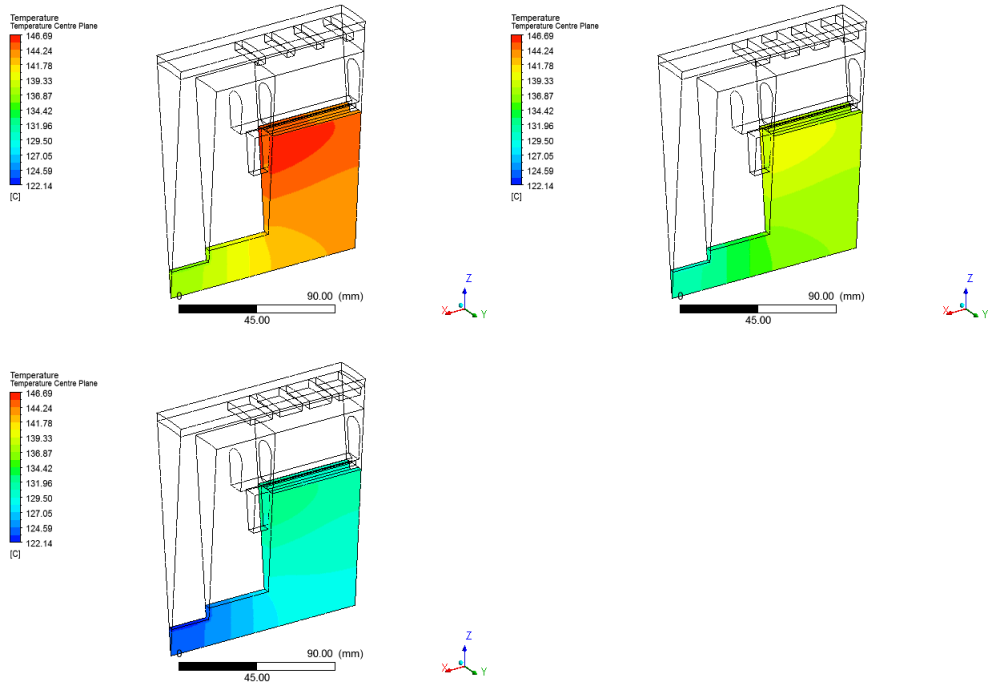

Figure 4.27 Temperature distribution in the surface of the rotor in different widths (Top Left: 5mm, Top Right: 10mm and Lower Left: 15mm)

Figure 4.27 shows the different temperature distribution of the rotor. These three pictures used the same indicator range with red colour at 146.69°C and blue colour at 122.14°C. Therefore, the colour represents the same criteria, and it can be seen that the temperature in the lower left picture is the lowest. Moreover, the patterns of the temperature distribution are the same. It distributed from the heat source (rotor conductor bar) to the stator, and it also distributed to the stator body.

Figure 4.28 shows the reason that the pattern of distribution can be shown in Figure 4.27. It can be seen that the 15 mm channel width has the lowest heat flux (the most minus value).

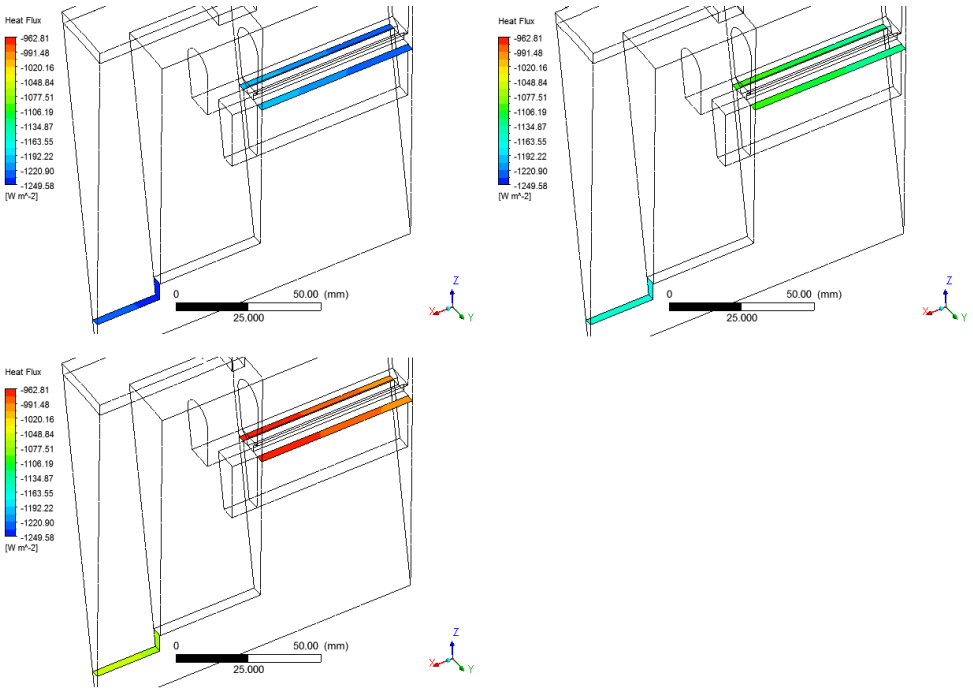

Figure 4.28 Heat Flux of Rotor Region in different widths

(Top Left: 5mm, Top Right: 10mm and Lower Left: 15mm)

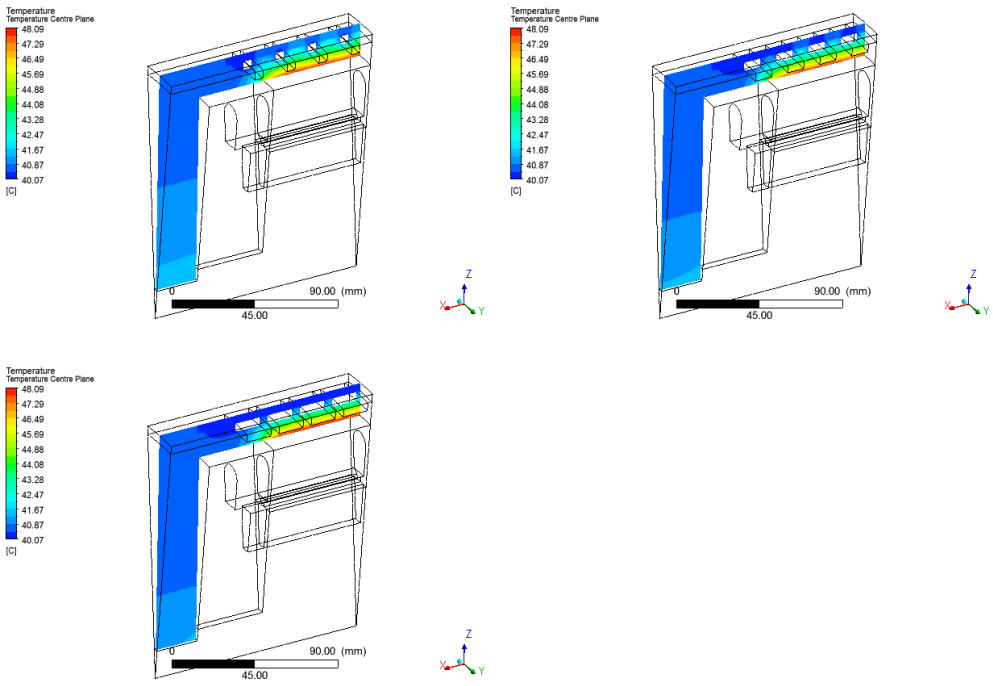

Figure 4.29 Temperature distribution in the surface of the rotor in different widths

(Top Left: 5mm, Top Right: 10mm and Lower Left: 15mm)

As same as, Figure 4.29 shows the temperature distribution in the stator body. In the area of the interface, the temperature of this field is the lowest in 15 mm. It was the results from the heat flux in the stator jacket as shown in Figure 4.30.

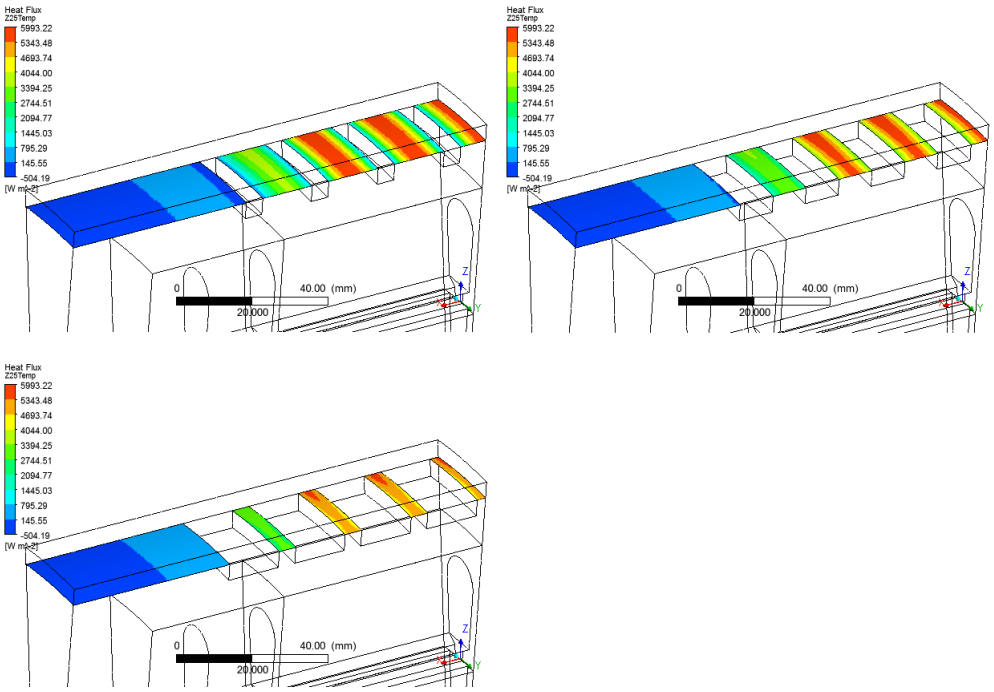

Figure 4.30 Heat Flux in (Blue) and out (Red) of Stator Jacket in different width (Top Left: 5mm, Top Right: 10mm and Lower Left: 15mm)

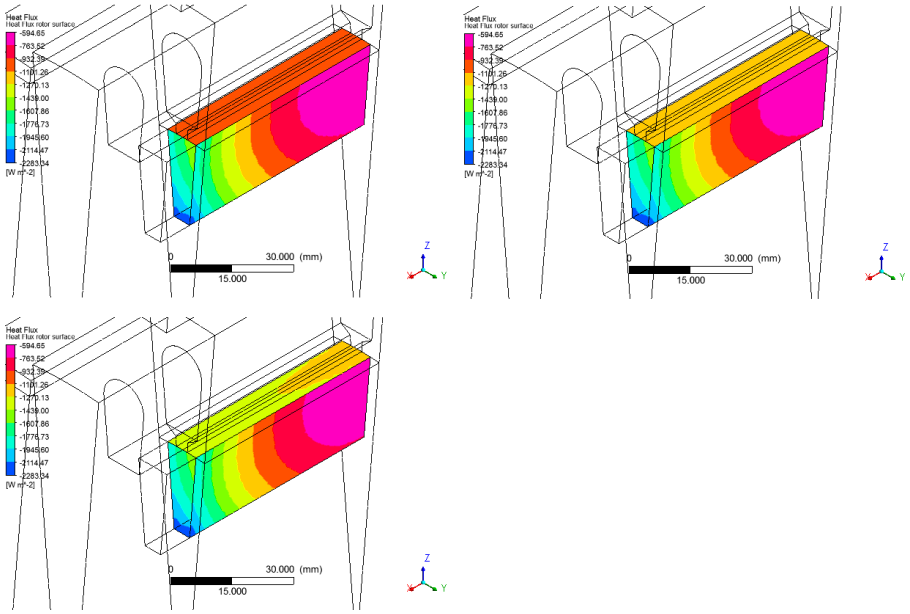

Figure 4.31 Heat Flux in direction out of Stator Jacket in different width (Top Left: 5mm, Top Right: 10mm and Lower Left: 15mm)

Therefore, when the rotor had low temperature, it means that the energy from the rotor bar can be transferred to the rotor easily. This is evidently shown in Figure 4.31. The rotor bar of the 15 mm width had the lowest (minus value) from the other left.

CHAPTER 5
CONCLUSIONS AND SUGGESTIONS

5.1 Conclusion

The objective of this studied was the pointing out an importance parameter that effect the electric motor cooling performance by using the ANSYS CFX software to assist the studied. Besides, this motor was used in the electric vehicle. Therefore, the temperature should not be only one criterion for concluding. However, the pressure drop should also be induced. The pressure drop is one of high importance to the electric vehicle energy management. If the pressure drop of the cooling system is greater than it supposed to be, that cooling system shall require the higher pump power to supply the cooling water. Additionally, this study was based on the worst case scenario that the motor was operated at the highest power or peak power, and the losses at peak power were assumed at 40% of peak power. Furthermore, the reliability of the study is only 75%. Then, the analysis result can be concluded that. 1) The most effective factor to the pressure drop is the width variation. However, in the normal operation the water flow rate shall be reduced to lower than 4 Litres per minute. It means that in 15mm model that Reynolds shall be reduced to lower than 7400. If it less than 4000, the state of flow will transform to transition and laminate, which it not good for the cooling performance. Moreover, the width variation model also shows, the wider duct is better for the cooling performance in the rotor and rotor conductor, but it was not effect to the temperature in the winding region. 2) If the cooling system were designed nearly the source, it would reduce the overall temperature of the motor except the rotor. Additionally, the distance between the rotor and the stator acts as insulation, and this insulation increases the difficulty energy exchange between these two objects. 3) The other one factor is the length of the cooling path. Hence, the variation of the pitch should be called as a path length adjusting or the cooling loop changing. The simplified mock-up, contain only three and four loops of the cooling duct. However, the loop did not effect to any particular components. The loop did only the rising and reducing of pressure drop, but the loop selection should be related to the channel width. For example, the 15

mm of the pitch should be not used for 15 mm channel width because the channel wall is removed. Then, 4) from taking the advantage of each investigation, the model can be created according to those results. The results shall be interpreted, the temperature of the simplified model and the completed model give similar results. The highest temperature located at the rotor region. However, many studied pay attention to the maximum temperature in the stator winding instead of the rotor bar. Beside that the primary failures of the electric motor is the thermal damage at the winding.

Finally, if the criterion was prioritised, it shall be ordered as following; 1) Operation temperature (losses minimise), 2) The width of the cooling channel (related to pressure drop). 3) The pitch of the cooling should be matched with channel width. The last, the most effective for temperature but cannot change is cooling base diameter, unless the base diameter variation is included in the electromagnetic study. Although the reliability of this study is only 75%, the verified method still made the impressive results. Therefore, this investigation can be used as guidance for the electric motor cooling system design. However, it should be re-calculated again, due to the difference of several parameters; for example the material, air gap, surface roughness.

5.2 Suggestion

The method and research methodology and validation, it might give this investigate more accuracy and more reliable. However, it might not be able to compare with the experiment. Once again, the results from this methodology are only being a guideline for making a new cooling system and awareness to the heat loss in each component. Besides, the motors have it own characteristic, so the temperature prediction should be considered every time that design the new motor. In term of analysis, it would be great if the analyse were done in a multi-physic study models.

REFERENCE

[1] Fuhs, A. E. (2009). *Hybrid vehicles and the future of personal transportation.* Boca Raton, Florida, USA: CRC Press.

[2] Wilson, D. S., & John, W. W. (1975). *RELIABILITY MODEL FOR MINIATURE BLOWERS PER MIL-B- 23071B.* New York: Shaker Research Corporation.

[3] Guo, W. &. (2009). Iron losses and transient temperature analysis of the permanent magnet synchronous motor for electric vehicles. *Electric machines and control* , 1, 017.

[4] Anonymous. (n.d.). IEC 60085, Electrical insulation – Thermal evaluation and designation.

[5] P.H., M., D., R., & D.R., T. (Sep 1991). Lumped parameter thermal model for electrical machines of TEFC design. *Electric Power Applications, IEE Proceedings B* , 205 - 218.

[6] Boglietti, A., Cavagnino, A., Lazzari, M., & Pastorelli, M. (Aug 2003). A simplified thermal model for variable-speed self-cooled industrial induction motor. *Industry Applications, IEEE Transactions on* , 945 - 952.

[7] Baggu, M., & Hess, H. (Sept. 2005). Thermal Modeling of “Direct Lamination Cooling (DLC)” Induction Motor for Hybrid Electric Vehicle Applications. *Vehicle Power and Propulsion, 2005 IEEE Conference* (pp. 468 - 472). Chicago: IEEE.

[8] Movahed, S., Farab Company, T. I., Oraee Mirzamani, S., Rajabi, A., & Daneshvar, H. (17-18 Feb. 2010). Estimation of insulation life of inverter- fed induction motors. *Power Electronic & Drive Systems & Technologies Conference (PEDSTC), 2010 1st* (pp. 335 - 339). Tehran, Iran: IEEE.

[9] Lee, Y., Lee, H.-B., Hahn, S.-y., & Lee, K.-S. (Mar 1997). Temperature analysis of induction motor with distributed heat sources by finite element method. *Magnetics, IEEE Transactions on (Volume:33 , Issue: 2)* , 1718 - 1721.

[10] Lampard, D., Dept. of Mech. Eng., N. U., Pickering, S., & Mugglestone, J. (15 Apr 1997). The use of computational fluid dynamics to model the air flow in the end region of a TEFC induction motor. *Modeling the Performance of Electrical Machines (Digest No: 1997/166), IEE Colloquium on* (pp. 2/1 - 2/5). London: IET.

[11] Ying, X., Technol., H. I., Weili, L., Shoufa, L., & Shumei, C. (6-8 Sept. 2006). Electromagnetic Field and Thermal Field Analysis and Simulation of an Induction Motor on Asymmetrical Operation Used in Electric Vehicles. *Vehicle Power and Propulsion Conference, 2006. VPPC '06. IEEE* (pp. 1 - 6). Windsor: IEEE.

[12] Nakahama, T., Suzuki, K., Hashidume, S., Ishibashi, F., & Hirata, M. (2006). Cooling airflow in unidirectional ventilated open-type motor for electric vehicles. *IEEE TRANSACTIONS ON ENERGY CONVERSION* , 645-651.

[13] Xiaochen, Z., Weili, L., Shukang, C., Junci, C., & Chunbo, Z. (2009). Thermal analysis of solid rotor in PMSM used for EV. *Vehicle Power and Propulsion Conference* (pp. 1637-1642). Dearborn, MI: IEEE.

[14] Jenwit Soparat, C.-n. B. (March 23-26, 2010). Computational Study of Totally Enclosed Fan Cooled System in an Electric Induction Motor. *The 14th International Annual Symposium on Computational Science and Engineering.* Chiang Rai, Thailand: ANSCSE.

[15] Cuiping, L., Yulong, P., Ronggang, N., & Shukang, C. (2011). Analysis of 3D static temperature field of water cooling induction motor in mini electric vehicle. *Electrical Machines and Systems (ICEMS), 2011 International Conference on* (pp. 1-5). Beijing: IEEE.

[16] BAPTISTA, B., MENDES, A., CRUZ, S., & CARDOSO, A. (2012). Temperature Distribution Inside a Three-Phase Induction Motor Running with Eccentric Airgap. *PRZEGLĄD ELEKTROTECHNICZNY* , 96-99.

[17] EL-Refaie, A. M., Harris, N. C., Jahns, T. M., & Rahman, K. M. (2004). Thermal Analysis of Multibarrier Interior PM Synchronous Machine Using Lumped Parameter Model. *IEEE TRANSACTIONS ON ENERGY CONVERSION , 19*, 303-309.

[18] Fan, J., Zhang, C., Wang, Z., & E.G., S. (2010). Thermal analysis of water cooled surface mount permanent magnet electric motor for electric vehicle. *Electrical Machines and Systems (ICEMS), 2010 International Conference on* (pp. 1024-1028). Incheon: IEEE.

[19] S.K, C., & P.K., B. (2010). A simple lumped parameter thermal model for electrical machine of TEFC design. *Power Electronics, Drives and Energy Systems (PEDES) & 2010 Power India, 2010 Joint International Conference on* (pp. 1-7). New Delhi: IEEE.

[20] Ehsani, M., Gao, Y., Gay, S. E., & Emadi, A. (2004). *Modern Electric, Hybrid Electric, and Fuel Cell Vehicles: fundamentals, theory, and design.* Boca Raton, Florida, USA: CRC PRESS.

[21] Larminie, J., & Lowry, J. (2003). *Electric Vehicle Technology Explained.* Chichester: John Wiley & Sons Ltd.

[22] X.D., X., K.W.E., C., & N.C., C. (2008). Selection of Electric Motor Drives for Electric Vehicles. *Power Engineering Conference, 2008. AUPEC '08. Australasian Universities* (pp. 1-6). Sydney, NSW: IEEE.

[23] Begamudre, R. D. (1988). *Electro-Mechanical Energy Conversion with Dynamics of Machines.* New Delhi, INDIA: Wiley Eastern Limited.

[24] Edward, T. J., & Kirk, A. J. (2003). The Fundamentals of AC Electric Induction Motor Design and Application. *INTERNATIONAL PUMP USERS SYMPOSIUM* , 95-106.

[25] Hugh D. Young, R. A. (2007). *University Physics.* (12, Ed.) San Francisco , California, USA: Pearson Addison-Wesley.

[26] Anonymous. (n.d.). Retrieved July 2, 2013, from Learn Engineering: http://www.learnengineering.org/

[27] Hughes, A. (2006). *Electric Motors and Drives - Fundamentals, Types and Applications.* Burlington: Elsevier Ltd.

[28] Anonymous. (2014, March). Rotating electrical machines – Part 30-1: Efficiency classes of line operated AC motors (IE code). *IEC 60034-30-1* . INTERNATIONAL ELECTROTECHNICAL COMMISSION.

[29] Cengel, Y. A. (2002). *Heat Transfer: A Practical Approach.* USA: McGraw-Hill Education.

[30] CENGEL, Y. A., & BOLES, M. A. (2006). *Thermodynamics; An Engineering Approach.* USA: McGraw-Hill Education (Asia).

[31] Munson, B. R., Young, D. F., & Okiishi, T. H. (2006). *Fundamentals of Fluid Mechanics.* USA: Wiley.

[32] Anonymous. (2011, November 21). Retrieved from Bergstrom Automotive: http://bergstromautomotive.blogspot.com/2011/11/charles-kettering-gm-first-engineering.html

[33] Mantilla, S. C. (2008). How the efficiency of induction motor is measured ? *The International Conference on Renewable Energies and Power Quality (ICREPQ '08).* Santander.

APPENDIX A

Preliminary Technical Drawing

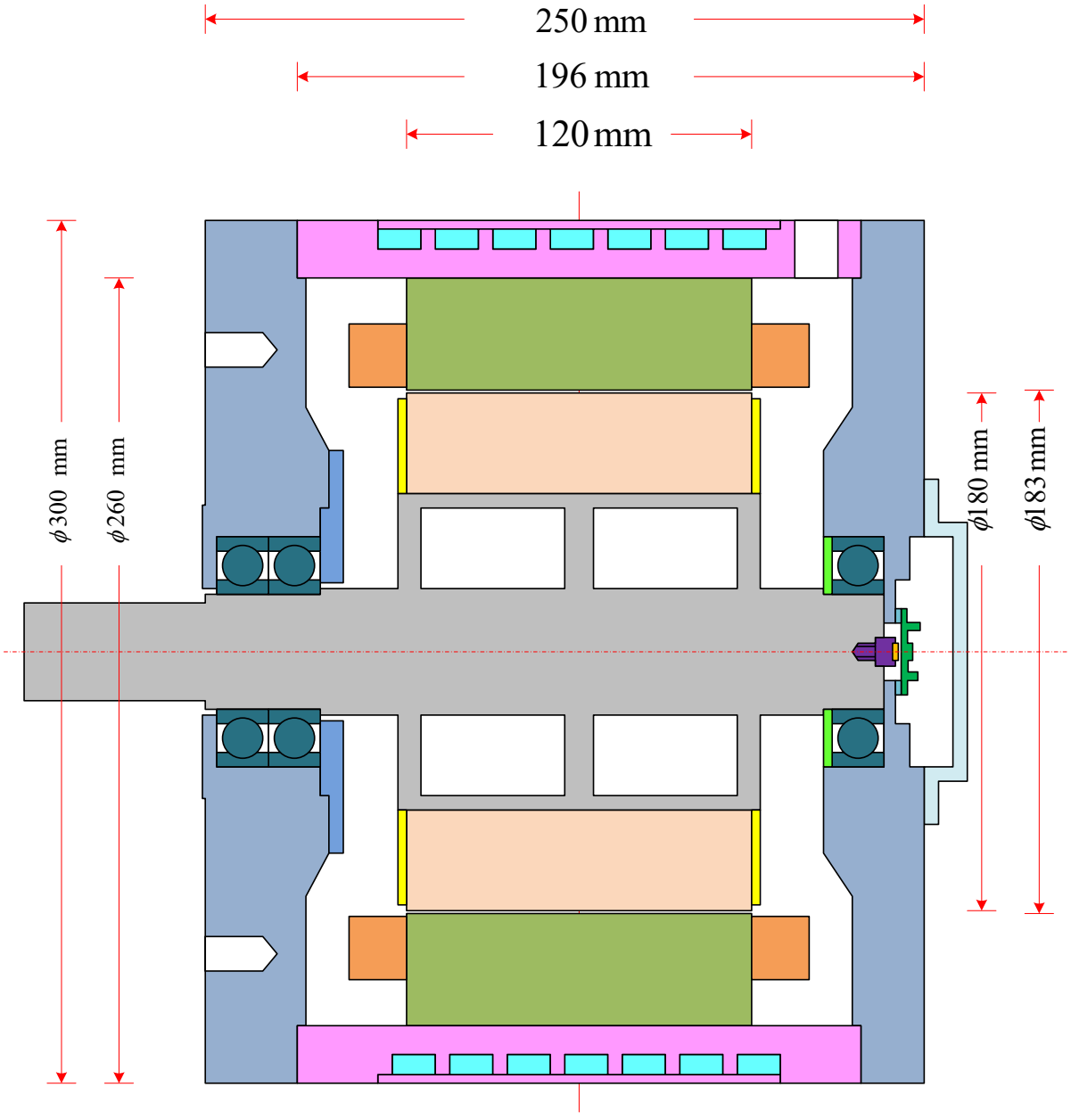

APPENDIX B

PROCEEDINGS

The Second TSME International Conference on Mechanical Engineering
19-21 October, 2011, Krabi

Effect of geometrical parameters towards the heat transfer in modified 80kW DC motor with radial water cooling duct.

Pongsatit Isarankura Na Ayuthaya[1], Jarruwat Charoensuk[1,*] and Chadchai Srisurangkul[2]

[1]Department of Mechanical Engineering, Faculty of Engineering, King Mongkut's Institute of Technology Ladkrabang, Bangkok, Thailand 10520

[2]National Metal and Materials Technology Center, Pathumthani, Thailand 12120

[*]Corresponding Author: kcjarruw@kmitl.ac.th, Tel: 0-2329-8351, Fax: 0-2329-8352

Abstract

One of the risks in using 80 kW DC induction motor as a prime mover for high performance vehicles is thermal failure due to cumulative heat generation from electrical loss. This unwanted heat could be taken out of the unit by a water coolant. This work deals with the effect of geometrical parameters on heat removal capability of the unit. The case of study can be divided into three parts. Part one is on the effect of cooling duct size. Part two is on the effect of base diameter and part three is on the number of cooling ducts. The model which has the best result among others is the 7.5 millimeter duct size with one cooling duct in the model of 30 centimeter of base diameter.

Keywords: DC Motor, Cooling, Three-dimensional, CFX, Heat transfer

1. Introduction

"In the future, the number of vehicles will grow up. If these vehicles are propelled by internal combustion engines, where will the oil come from?"[1]. This is a big question for the industrial community which is heavily dependent on energy. Moreover, global warming has become a social issue; the environmental protection and energy consumption are the most popular topics for those who are concerned about the earth. At that point many researchers try to look for technologies which are cleaner and more efficient than conventional ones.

The technologies of future vehicles are developed in many countries from many companies. There are many components that must be developed, especially the driving system, which focus on how to increase the efficiency.

The performances of an electric vehicle are usually shown in terms of acceleration performance and energy consumption. The acceleration performances are starting acceleration, passing ability and maximum speed. In an electrical vehicle, only electric motor delivers torque to the driven wheels. Thus the vehicle performance is completely determined by the torque speed or power-speed characteristic of the electric motor. In order to achieve these requirements, it needs to improve

the motor characteristic especially energy consumption [2].

It is well known that the DC motor is not a perfect energy conversion device. It also generates four major losses which are (1) heat generation by ball bearings, (2) heat generation by the electric motor in rotor and stator "Fig. 1", (3) heat generation due to viscosity shear of air by the rotating components of the spindle, and (4) qualitative description of power distribution from spindle heat sources to heat sinks [3]. These heat losses will increase the energy consumption and it also cause damages directly to the induction wire of the motor. At that point the heat loss can be damaging to the motor. These heat losses must be removed from the motor.

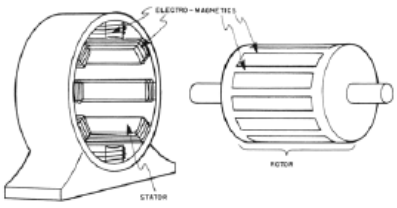

Fig. 1 The stator and rotor of electric motor

2. Problem Specification

2.1 Problem

One of the risks in using 80 kW DC induction motor as a prime mover for high performance vehicles is thermal failure due to cumulative heat generation from electrical loss. This unwanted heat could be taken out of the unit by a water coolant.

2.2. Investigation

Aim of this research is to study an effect of temperature distribution and pressure drop which depend on geometry of the motor housing. This research can be divided into three parts. Part one concerns about the effect of cooling duct size. Part two is on the effect of base diameter and part three is the number of cooling ducts.

2.2. Assumption

According to EU regulation (IE2: High efficiency), the motor must have minimum efficiency of 95%. For safety reason, this study has adopted heat loss at 10% or 8 kW instead of 5% [4].

3. Mathematical Models

The energy conservation in the system is determined using the energy balance equation (Eq.1).

$$E_{in} - E_{out} = \Delta E_{system} \quad (1)$$

Heat flux generated by heat loss is determined by equation (2), when $\dot{Q}_{loss}$ is determined by equation (3).

$$q'' = \frac{\dot{Q}_{loss}}{A} \quad (2)$$

$$\eta_{th} = \frac{\dot{W}_{net}}{\dot{E}_{in}} = \frac{\dot{W}_{net}}{\dot{W}_{net}+\dot{Q}_{loss}} \quad (3)$$

Equation (4) of thermal energy is used for calculation of total heat rejection of cooling water.

$$\dot{Q} = \dot{m}_c c_{pc}(T_{c,out} - T_{c,in}) \quad (4)$$

Equation (5) is used for explaining the simple phenomena of heat resistance and temperature distribution of motor housing next to cooling duct at base diameter described in section (5.1.2) [5].

$$\dot{Q} = (2\pi L)\frac{T_1 - T_2}{\ln(r_2/r_1)} \quad (5)$$

Equation (6) is used for explaining the simple phenomena of pressure drop which is described in section (5.2) **[6]**.

$$\Delta P = \overline{\gamma} h_L \quad (6)$$

$$h_L = h_{L\,major} + h_{L\,minor} \quad (6a)$$

$$h_{L\,major} = f\frac{l}{D}\frac{v^2}{2g} \quad (6b)$$

$$h_{L\,minor} = K_L\frac{v^2}{2g} \quad (6c)$$

4. Research methodology

4.1. Case study

The study on effects of (1) duct sizing, (2) base diameter and (3) number of ducts in 20 millimeters of ring width are described as follow.

4.1.1 Cooling duct size

The red box on the cross-section view of cooling duct as seen in "Fig. 2b" shows sizing of cooling duct which have five mm of height and "x" mm of width. In this case study, the "x" value varies from 5, 7.5, 10, 12.5, 15 to 17.5 mm.

4.1.2 Cooling duct location

This case focuses on the effect of base diameter in terms of temperature distribution when the black line in "Fig. 2a" is the base diameter of the cooling duct. In this case, 7.5 mm. width and 5 mm. height of duct size is used and base diameter is varied from 30, 32 to 34 cm.

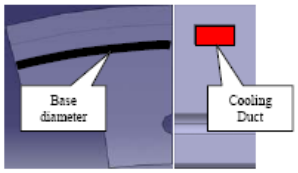

(a) (b)

Fig. 2a Front view of cooling duct (15 mm.).

Fig. 2b Cross-section view of cooling duct.

4.1.3 Number of cooling duct per ring

In section 4.1.1 and 4.1.2 only base diameter and duct size are varied but the number of cooling ducts remains the same as one cooling duct. In this case, the effect of the number of cooling ducts is studied by using 1-duct model compare with 2-duct model. Both models contain 5 mm width of cooling duct size and 20 mm of ring width "Fig. 3".

Fig. 3 Cross-section at 2 cooling duct model

4.2. Computation procedure

The study on effective parameter in terms of temperature distribution in each case requires a commercial program code name "CFX ANSYS 12" as a tool for analysis.

By using the CFX program, a domain of solid and fluid must be set up. Steel is used as a solid domain and water at 25℃ is used as a fluid domain. For boundary condition, it can be divided into three zones, first zone is heat source (1), second is symmetry (2) and the last one is adiabatic wall zones "Fig. 4"

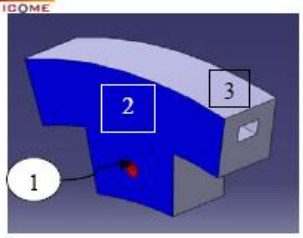

Fig. 4 Zones of boundary condition

By assuming the heat source was generated in the middle of the teeth, Zone 1 in "Fig. 4" shows a heat source which is set up in the program as a heat flux wall, when the value of heat flux is 212,210 W/m^2 or 66.67 W per heat source zone.

In terms of fluid domain, the boundary condition of cooling water flow is to have inlet at pole no.12 and outlet at pole no.6 as seen in "Fig. 5". The flow rate and temperate at inlet port are 0.1 kg/s and 60℃ and the pattern of flow is turbulent and the reason is shown in table 1.

Table 1 the flow pattern in each cooling duct size.

Size (mm)	Velocity (m/s)	Reynolds number	Flow Pattern
5.0	2.00	2.11E+04	Turbulent
7.5	1.33	1.69E+04	Turbulent
10.0	1.00	1.41E+04	Turbulent
12.5	0.80	1.20E+04	Turbulent
15.0	0.67	1.05E+04	Turbulent
17.5	0.57	9.37E+03	Turbulent

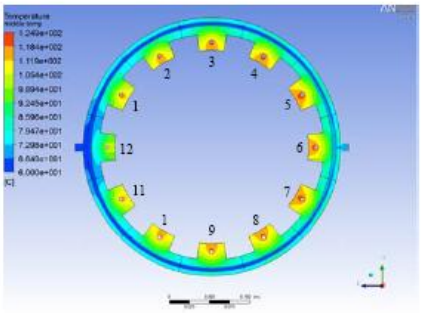

Fig. 5 The located of the pole.

5. Result and Discussion

5.1. Results

5.1.1. Cooling duct size

In a 5-mm cooling duct size model, it was found that the temperature was 60℃ at the entrance of inlet port and the temperature rose to 61.88℃ when it flowed out of channel. The profile of temperature distribution is shown in "Fig. 6".

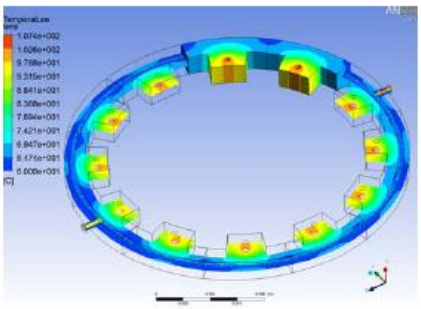

Fig. 6 Temperature distribute in the middle of cooling duct (5mm.)

From "Fig. 6" the highest temperature are pole no.5 and pole no.7. At this point "Fig. 7" the temperature is 94.41℃.

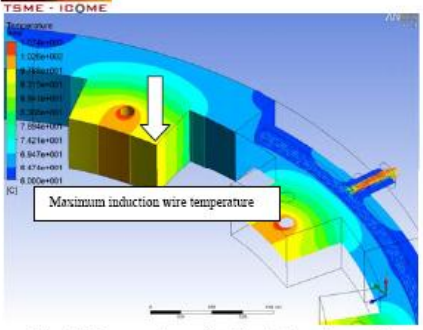

Fig. 7 Temperature distribute in pole no.5 (5mm.)

At the cross-section of the cooling duct "Fig. 8", it was found that the changes of temperature profile between cooling duct wall and ring boundary had a low temperature region located at the cooling duct wall and the temperature increased to its peak at ring boundary.

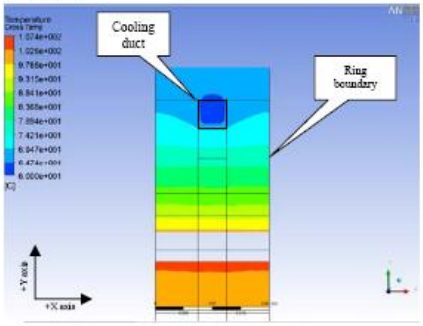

Fig. 8 Temperature distribute in the cooling duct cross-section.

The temperature profile is the same for the other models with small differences. Table 2 shows a result in details.

5.1.2. Cooling duct base diameter

In this part, the profiles of temperature distribution are similar to 7.5-mm cooling duct size model studied in section 5.1.1. But the pole no.5 and no.7 of 30-cm, 32-cm and 34-cm base diameter of cooling duct have 95.11, 101.65 and 108.79 respectively. The result of this part can be explained in Table 3 and the profile of temperature in 34-cm base diameter of cooling duct which has a maximum temperature at pole no.5 and pole no.7 is shown in "Fig. 9".

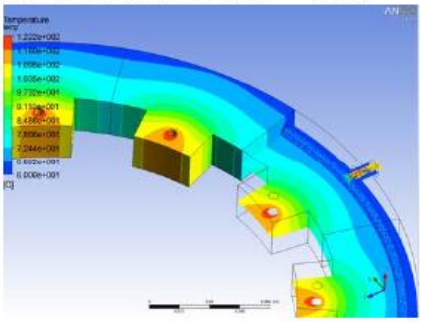

Fig. 9 Temperature distribute at pole no.5 (34cm.)

According to "Eq. (5)", if the base diameter is increased from 30 cm to 32 cm or 34 cm, the heat flow resistance will be increased too.

Table2 the simulation results in term of cooling duct sizing at 0.1kg/s of cooling water mass flow rate.

Descriptions	Duct size (mm.)					
	5.0	7.5	10.0	12.5	15.0	17.5
Pressure drop (kPa.)	23.63	22.29	23.43	23.54	24.03	23.68
Maximum temperature at pole no.5 and no.7 (C.)	94.41	95.12	95.65	96.42	97.34	99.21
Outlet coolant temperature (C.)	61.88	61.89	61.89	61.87	61.87	61.88
Heat reject (W.)	0.786	0.790	0.790	0.782	0.782	0.786

Table 3 the simulation results in term of base diameter at 0.1kg/s of cooling water mass flow rate.

Descriptions	Base diameter (cm.)		
	30	32	34
Pressure drop (kPa.)	22.29	21.77	22.00
Maximum temperature at pole no.5 and no.7 (C.)	95.11	101.65	108.79
Outlet coolant temperature (C.)	61.89	61.9	61.9
Heat reject (W.)	0.79	0.794	0.794

5.1.3. Number of cooling duct per ring

The result of 1-cooling-duct model and 2-cooling-duct model provides a significant difference because in 2-cooling-duct model the distance between ducts is shorter than 1-duct model by half. The temperature distributions in cross-section for both models are shown in "Fig. 10" and "Fig. 11". The result of this case can be explained in Table 4.

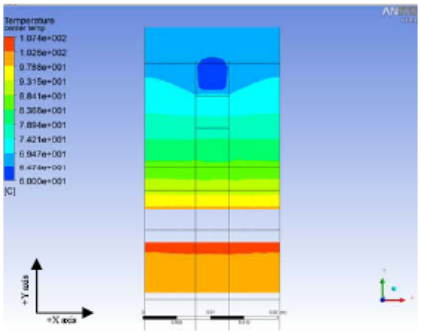

Fig. 10 Cross-section temperature distribution of one duct model.

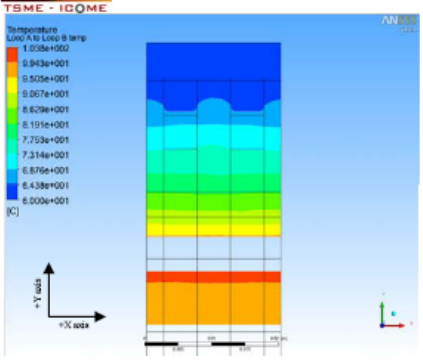

Fig. 11 Cross-section temperature distribution of two duct model.

Table 4 the simulation results in term of number of cooling duct at 0.1kg/s of cooling water mass flow rate.

Descriptions	Number of cooling duct	
	1	2
Pressure drop (kPa.)	23.63	22.59
Maximum temperature at pole no.5 and no.7 (C.)	94.41	89.45
Outlet coolant temperature (C.)	61.88	60.94
Heat reject (W.)	0.786	0.786

5.2 Discussion

According to the results in section "5.1.", many data show the advantages and disadvantages in each case study (section "5.1.1.", "5.1.2." and "5.1.3."). In section "5.1.1.", according to "Eq. (6) - (6c)" The temperature deferential of cooling water between inlet temperature and outlet temperature are small. Therefore, the effect of density due to the temperature is negligible and the pressure is decreased when duct size is increased but in Table 1 the pressure drop in each duct size does not vary in linear function with size of channel flow due to domination of minor loss. In this case, there are 2 types of pressure drop. First is major loss and the other is minor loss. For a major loss the main factor is the size but the difference is small. It can be assumed that this major loss provides only small influences. For a minor loss, it relates to an increase in area (pole no.12), a decrease in area (pole no.6), 3-way and Bending in circle. The minor loss will be increased, if the size of duct is increased. It will be convenient if the area of inlet port can be adjustable for decreasing pressure drop in these areas. For a maximum temperature at pole no.5 and pole no.7, it was found that when the duct size is increased the temperature will be increased too, because velocity of water will decrease. It can be concluded that temperature is strongly related to water speed.

In section "5.1.2.", the maximum temperature at pole no.5 and pole no.7 in table 3 increases if the base diameter is increased, its relationship can be explained in "eq. (5)".

When compare between "Fig. 10" and "Fig.11" in section "5.1.3.", the profiles of temperature are not the same. In "Fig. 11" low temperature zone is larger than that in "Fig. 10" because it is easier to control a temperature around cooling duct wall in model of 2 cooling ducts. When considering about temperature distribution in cross-section the temperature will be increased along thickness of ring ("+X" and "-X" axis), so that if the model has many cooling ducts, it is easy to control a temperature profile at the middle of both ducts in condition of multi-cooling ducts model.

6. Conclusion

In this study, it can be concluded for 5 mm of inlet port of 7.5 mm with one cooling duct in 30 cm of base diameter gives the best result for this research.

7. Acknowledgement

Special thanks to National Metal and Materials Technology Center.

8. References

8.1 Article in Journals

[1] C.C. Chan, K.T. Chau, "Modern electric vehicle technology", *engineering philosophy of EV development*, pp. 1.

[2] M. Ehsani, Y. Gao, and S. Gay, "Characterization of Electric Motor Drives for Traction Applications", *IEEE paper, ISBN: 0-7803-7906-3 This paper appears in: Industrial Electronics Society*, Vol.1, pp.891, 2003.

[3] C.H. Huang, H.C. Lo, "A three-dimensional inverse problem in estimating the internal heat flux of housing for high speed motors", *Applied Thermal Engineering* 26 (2006) 1515–1529

8.2 Books

[4] James Larminie, John Lowry, "Electric Vehicle Technology Explained", ISBN 0-470-85163-5, pp.176

[5] Yunus A. Çengel, "Heat Transfer: A Practical Approach", 2nd edition, pp. 46, 49, 679.

[6] Bruce R. Munson, Donald F. Young, Theodore H. Okiishi, "Fundamentals of Fluid Mechanics", 5th edition, ISBN-10: 0-471-72578-1, pp. 430, 432, 437.

AUTHOR BIOGRAPHY

NAME Mr. Pongsatit Isarankura Na Ayuthaya

DATE OF BIRTH 26 February 1988, Bangkok, Thailand

ADDRESS 590 Mou.10, North Samrong, Mueang Samut Prakan
Samut Prakan Province, 10270

EDUCATIONAL BACKGROUND

2015 - 2010	M.Eng . in Automotive Engineering (International program), International College, King Mongkut's Institute of Technology Ladkrabang (KMITL), Thailand
2010 – 2006	B.Eng . in Mechanical Engineering King Mongkut's Institute of Technology Ladkrabang

SCHOLARSHIPS

2012 – 2010	TAIST-Tokyo Tech scholarship, the Master's Degree in Automotive Engineering funded by National Science and Technology Development Agency (NSTDA), Thailand

EXPERIENCES

Present – 2014	Design Engineer (Exterior), Rolling Stock division at Bombardier Transportation Signal (Thailand).
Mar 2014 - July 2012	Staff Engineer (Design Engineer), Body design division at NISSAN MOTOR ASIA PACIFIC

Publications

1) Isarankura P., Charoensuk J., and Srisurangkul C. "Effect of geometrical parameters towards the heat transfer in modified 80kW DC motor with radial water cooling duct." The 2nd TSME International Conference on Mechanical Engineering, Krabi, Thailand.